CFD Letters

Journal homepage:
https://semarakilmu.com.my/journals/index.php/CFD_Letters/index
ISSN: 2180-1363

Improve Analytical Solutions for Trapezoidal, Rectangular and Dovetail Shapes of Inclined Longitudinal Porous Fin

Ahmed R Khlefha[1*], Abeer Majeed Jasim[2]

[1] Department of Mathematics, College of Science, University of Basrah, Iraq
[2] Department of Mathematics, College of Science, University of Basrah, Basrah, Iraq

ARTICLE INFO

Article history:
Received 20 August 2023
Received in revised form 25 September 2023
Accepted 21 October 2023
Available online 31 August 2024

Keywords:
Natural convection; fully wet fin; differential transform method; Galerkin method; least squares method

ABSTRACT

This study improved the approximate analytical solutions of the heat distribution and transport of inclined longitudinal porous fin in the presence of radiative and convective environments with rectangular, trapezoidal, and dovetail profiles. The model of Darcy, which mimics the interaction of fluids and solids, is utilized to obtain the equation of governing the heat transfer of the porous fin. To investigate the rectangular, trapezoidal, and dovetail profiles, a single equation has been solved through analysis of the mathematical model by using the optimal differential transform method (ODTM) which consist least squares differential transform method (LSDTM), and the Galerkin differential transform method (GDTM) while the BVP4c presents the numerical solution. A comparison is made between the approximate analytical and numerical solutions for different parameters. It results in that the solutions produced from LSDTM and GDTM are closer to the numerical solution than the solutions of DTM, nonlinear autoregressive exogenous-levenberg marquardt algorithm (NARX-LMA) and cascade feedforward backpropagated-levenberg marquardt algorithm (CFB-LMA). A comprehensive graphic analysis was conducted to examine the effect of variation in inclination angles, tapering at the tip, wet porous parameters, internal heat generation, progressive natural convection parameters, and dimensionless radiation parameters on the thermal profile and thermal transfer rate of the porous longitudinal fin. The split fin design achieves the greatest heat transfer rate, trailed by rectangular and trapezoidal fin profiles, assuming that internal heat generation is maintained to a minimum.

1. Introduction

Heat transfer research, which aims to give the best thermal performance in incredibly tiny quantities, has seen an increase in interest because of the increased need for device downsizing in a range of applications. As a result, the rate of heat transfer per unit of volume increases significantly, making it possible to fabricate smaller parts for a variety of technical applications, including thermal energy storage, aerospace engineering, solar collectors, thermal regulation of electronic components, and heat exchangers [1]. Nield and Bejan [2] found that the application of longer

* *Corresponding author.*
E-mail address: arkdsh85@gmail.com (Ahmed Rasheed Khlefha)

https://doi.org/10.37934/cfdl.17.1.140161

surfaces and porous media are two efficient methods for increasing heat transfer. Porous fins have been employed in many applications because they combined the benefits of both of these methods, increasing the ratio of volume to heat transfer area [3, 4]. Utilizing porous fins has several advantages, but the main one is that they increase the fin's useful surface area, allowing it to exchange the working fluid with heat. Furthermore, when the solid material is taken out, the porous fin's effective heat conductivity falls. By expanding the effective surface area, the issue can be solved. The extending surface can be made up from both porous surfaces and solid; when exposed right away, heat from the solid surface interacts with its surroundings. Using this physical fact as motivation, the same author carried out a second investigation into the impact of radiation heat transfer and condensation on heat transmission through a porous extended surface by Kiwan [5]. Kundu and Bhanja [6] expanded Kiwan's work in order to create a precise mathematical model for performance analysis of the fins using the domain decomposition method (ADM), taking into account the prior advances. The best-case scenario analysis of the rectangular porous fin was also looked at from an operational standpoint. When the need for heat dissipation rate is sufficiently high, it is advised to use a porous fin. Several prediction models were presented based on comparative evaluations to identify a better model to study a fin. Additionally, a construct T-shaped porous fin's thermal performance and temperature spread were explored by Gorla and Bakier [7]. Petroudi *et al.,* [8] studied the dissipation of energy from a porous fin to develop a non-linear model of the heat transport in straight porous fins using the homotopy perturbation method. A porous fin is used to create a non-linear model for the heat transfer in straighter porous fins in order to determine the maximal heat transfer in porous fins with various profiles, including rectangular, convex, and exponential shapes. Kundu *et al.,* [9] employed ADM to calculate maximum heat transfer in porous fins with different profiles, such as rectangular, convex, and exponential forms. Abdulridah and Jasim [10] their research focused on analyzing the fluid dynamics and thermal properties of a nanofluid within a porous medium, following the Jeffrey Hamel flow problem}. Their research's key result is that exponential profiles with negative power factors transmit heat at a rate that is much higher than that of rectangular profiles and just marginally higher than that of convex profiles. In their study, the importance of radiative heat loss was assessed and covered. Through using temperature-dependent conductive, radiative, and convective heat transfer coefficients. Aziz and Torabi [11] quantitatively investigated the fin problem. Atouei *et al.,* [12] contrasted the collocation approach with the Least squares method in order to determine the thermal profile of a semi-spherical fin with thermal characteristics and nonuniform heat generation. Patel and Meher [13] utilized the domain decomposition Sumudu transform method (ADSTM) to derive analytical solutions for a fractional order energy balance equation relating to efficiency along and heat distribution with temperature-dependent generation of thermal conductivity and internal heat. Jawairia and Raza [14] used the optimization technique response Surface method (RSM), a permeable fin used in aerospace engineering to conduct a sensitivity analysis of radiation transmission and natural convection. Roy *et al.,* [15] employ the finite difference technique (FDM) to examine the effects of electric and magnetic field concentrations on the longitudinal porous fin's heat transfer coefficient, generation of heat, and surface emissivity. Each of the strategies previously mentioned has its own unique potential, sensitivity, efficiency, and accuracy as well as defects, shortcomings, and disadvantages relative to the others. A number of these methods have been thought of as gradient-based ones, and therefore need knowledge of the problem beforehand. Prior knowledge involves the initial guess decision, small variables, differentiability, and smoothing of this problem. In particular, the semi-analytical method has emerged in recent years to analyse fluid flow issues [16]. An example of this method is the differential transformation method (DTM). Many researchers chose to utilize this method to solve the nonlinear equations due to its benefits and capabilities. Zhou [17] created DTM, which has

proven to be one of the most effective and well-established techniques. DTM was applied by Kundu *et al.,* [18] to study the thermal analysis of exponential fins under sensible and latent heat transfer. Sowmya and Gireesha [19] used DTM to perform an approximate solution in Taylor's series form for the heating pattern of structured straight permeable fins and circular permeable fins with internally generated surface heat. Khudir [20] has applied the fractional differential Transform Method (FDTM) to solve irrational order fractional differential equations. Hussin *et al.,* [21] utilized the differential transform approach to get solitary wave solutions. Varun Kumar *et al.,* [22] analysed the temperature distribution and thermal stresses within an annular fin that has internal heat generation and is exposed to multi-boiling heat transfer by using the differential transform method. Sabdin *et al.,* [23] introduced an updated version of the modified r differential transformation method to derive a semi-analytical approximation for nonlinear telegraphic equations (NLTEs) with a source term. Yaghoobi and N Torabi [24] employ DTM to solve nonlinear problems, and the correctness of their solutions was confirmed by comparing their findings to those obtained using alternative methods. Kotnurkar and Beleri [25] apply the differential transformation method to derive solutions for non -linear partial differential equations. Hussin *et al.,* [26] introduced modified reduced differential transformation method, it was utilized to address the nonlinear forced Korteweg-de Vries equations. The aim of this work study heat distribution and the heat transfer within the fin for the mathematical model of an inclined longitudinal porous fin of different profiles in the presence of convective and radiative environments. Furthermore, a machine learning strategy is utilized to study temperature distribution in the fin. The use of the design of ODTM to avoid the nonlinearity of the complex systems like mass and heat transfer problems of the longitudinal porous fin with different profiles with the same settings. Moreover, the influence of variations in tip tapering, inclination angle, porous wet parameter, porosity, internal heat generation, dimensionless radiative parameter, and progressive natural convective parameter on heat transfer rate and thermal profile for the fin is investigated. The numerical solutions obtained from BVP4c the comparison with the solutions extracted from DTM, LSDTM, and GDTM. Also, the results obtained by LSDTM are compared with NARX-LMA and CFB-LMA.

2. Methodology

Consider about a longitudinal porous fin with a set width$W$, length L, and bases thickness t_b that is connected to a surface with an inclination angle ε. The interaction of porous medium and the fluid is enhanced by the inclination of a fin, increasing thermal efficiency as the heat sink's length-to-height ratio drops. Figure 1 - Figure 3 illustrates the many longitudinal fin profiles (dovetail, rectangular and trapezoidal) that may be created by adjusting the fin tip. A porous fin's base is maintained at a constant temperature $\overline{T}_b$, while the temperatures of the convective and radiative heat sink nearby are $\overline{T}_c$ and $\overline{T}_s$, respectively. It is believed that the internal heat production is a linear function of temperature. A number of assumptions are taken into account when performing the analysis. It is these assumptions, the fin's medium is homogeneous, porous, isotropic, and filled with a single-phase fluid, as well using a porous media and a fluid, Darcy's law models this interaction, in addition to only the axial orientation causes the fin's internal temperature to change. Additionally, fluctuations in surface radiation and the non-axial axis Drainage in the fins are disregarded, Fin is completely submerged in fluid, and there is a local thermodynamic equilibrium between the solid and the liquid, and then Temperature affects both the convective and radiative heat transfer coefficients. This process is adiabatic because there is less heat transfer across the tip of the fin compared to heat transfer at the side surface. Finally, the environment in which the fin operates is stable. The general equation of the steady state for the energy transfer fin problem in the above-mentioned assumptions can be expressed [13] as follows:

$$\tilde{q}_{\bar{x}} - \tilde{q}_{\bar{x}+d\bar{x}} + \tilde{q}^*(\bar{T})t(\bar{x})Wd\bar{x} - 2\bar{m}C_p(\bar{T} - \bar{T}_a) - 2\eta(\bar{T})\sigma Wd\bar{x}(\bar{T}^4 - \bar{T}_s^4) - 2h_D\, Wd\bar{x}i_{fg}\left(1 - \tilde{\phi}\right)(\tilde{w} - \tilde{w}_a) - 2h\,(\bar{T})Wd\bar{x}\left(1 - \tilde{\phi}\right)(\bar{T} - \bar{T}_a) = 0 \quad (1)$$

here, $\tilde{q}_{\bar{x}}$ represents the rate of heat transfer in the axial direction of the fin, h the heat transfer coefficient, $\bar{T}_a$the ambient temperature, $\tilde{q}^*$ the internal rate of heat generation, η is the surface emissivity of the fin, $\bar{T}$ the local fin temperature, i_{fg} the latent heat of water evaporation, C_p is the specific heat at constant pressure, and h_D the uniform mass transfer coefficient. $\tilde{w}$ and $\tilde{w}_a$ the relative humidity ratio of the saturated and surrounding air, respectively. Fourier's law in conduction describes the rate of heat transfer at the base of the fin represented by $\tilde{q}$ as follows:

$$\tilde{q} = -K_{eff}A(\bar{x})\frac{d\bar{T}}{d\bar{x}}, \quad (2)$$

Where $A(\bar{x})$ and K_{eff} are the cross-sectional area of a porous fin at distance $\bar{x}$ and effective thermal conductivity, which are defined

$$K_{eff} = \left(1 - \tilde{\phi}\right)K_s + \tilde{\phi}K_f, \quad (3)$$

And

$$A(\bar{x}) = Wt(\bar{x}), \quad (4)$$

Where K_s and K_f reflect the thermal conductivity of the solid and fluid, respectively. $\tilde{\phi}$ signifies the porosity. $\left(1 - \tilde{\phi}\right)$ represents the effective surface of the solid and $t(\bar{x})$ is the fin thickness. Additionally, $\bar{m}$ is the mass of fluid passing through a porous fin, which is designated [27] as;

$$\bar{m} = \rho_f v(\bar{x})Wd\bar{x}, \quad (5)$$

The fluid's velocity in the porous fin is provided as in Darcy's model by the following equation:

$$v(\bar{x}) = \frac{gK\tilde{\beta}_f(\bar{T} - \bar{T}_a)\sin(\varepsilon)}{v_f}, \quad (6)$$

The definition given by Ghasemi *et al.,* [28] assumes the internal heat production of the fin varies linearly with the surface temperature

$$\tilde{q}^*(\bar{T}) = \tilde{q}_a^*\left(1 + \eta_g(\bar{T} - \bar{T}_a)\right), \quad (7)$$

Assumed to be functions of temperature, the fin surface's emissivity η and coefficient of convective heat transfer h are given as,

$$h(\bar{T}) = h_a\left(\frac{\bar{T} - \bar{T}_a}{\bar{T}_b - \bar{T}_a}\right)^m = C_p h_D \tilde{L}e^{\frac{2}{3}}, \quad (8)$$

$$\eta(\bar{T}) = \eta_s\left(1 + \tilde{\beta}(\bar{T} - \bar{T}_s)\right), \quad (9)$$

Heat transfer coefficient at temperature $\bar{T}_a$ is represented by h_a , Lewis number is represented by Le, surface emissivity of a fin at temperature $\bar{T}_s$ is represented by η_s, and surface emissivity fluctuations with temperature $\bar{T}$ is measured by $\tilde{\beta}$. The non-linear ordinary differential equation (ODE) governing the temperature distribution in the fin is obtained by substituting Eq. (2) – Eq. (9) in Eq. (1) as follows:

$$K_{eff}\frac{1}{d\bar{x}}\left(t(\bar{x})\frac{d\bar{T}}{d\bar{x}}\right)-\frac{2\rho_f g K C_p\tilde{\beta}_f\sin(\varepsilon)}{\tilde{v}_f}(\bar{T}-\bar{T}_s)^2+\tilde{q}_a^*\left(1+\eta_g(\bar{T}-\bar{T}_a)\right)t(\bar{x})-\frac{2h_a\, i_{fg}(1-\tilde{\phi})(\tilde{w}-\tilde{w}_a)(\bar{T}-\bar{T}_a)^m}{C_p\tilde{L}e^{\frac{2}{3}}(\bar{T}_b-\bar{T}_a)^m}-$$
$$\frac{2h_a\,(1-\tilde{\phi})(\bar{T}-\bar{T}_a)^{m+1}}{(\bar{T}_b-\bar{T}_a)^m}-2\sigma\eta_s\left(1+\tilde{\beta}(\bar{T}-\bar{T}_s)\right)(\bar{T}^4-\bar{T}_S^4)=0, \tag{10}$$

The semi-local thickness of the longitudinal fin is different for different profiles.

$$t(\bar{x})=t_b-\tilde{\delta}\left(\frac{\bar{x}}{L}\right), \tag{11}$$

Where the profile is based on δ. Eq. (11) Substituted into Eq. (10), we get

$$K_{eff}\frac{1}{d\bar{x}}\left(\left(t_b-\tilde{\delta}\left(\frac{\bar{x}}{L}\right)\right)\frac{d\bar{T}}{d\bar{x}}\right)-\frac{2\rho_f g K C_p\tilde{\beta}_f\sin(\varepsilon)}{\tilde{v}_f}(\bar{T}-\bar{T}_s)^2+\tilde{q}_a^*\left(1+\eta_g(\bar{T}-\bar{T}_a)\right)\left(t_b-\right.$$
$$\left.\tilde{\delta}\left(\frac{\bar{x}}{L}\right)\right)-\frac{2h_a\, i_{fg}(1-\tilde{\phi})(\tilde{w}-\tilde{w}_a)(\bar{T}-\bar{T}_a)^m}{C_p\tilde{L}e^{\frac{2}{3}}(\bar{T}_b-\bar{T}_a)^m}-\frac{2h_a\,(1-\tilde{\phi})(\bar{T}-\bar{T}_a)^{m+1}}{(\bar{T}_b-\bar{T}_a)^m}-2\sigma\eta_s\left(1+\tilde{\beta}(\bar{T}-\bar{T}_s)\right)(\bar{T}^4- \tag{12}$$
$$T_S^4)=0$$

And the corresponding boundary conditions are given by

$$\bar{T}=\bar{T}_b\,,\quad \text{at}\qquad \bar{x}=0, \tag{13a}$$

$$\frac{d\bar{T}}{d\bar{x}}=0,\quad \text{at}\qquad \bar{x}=L, \tag{13b}$$

The following dimensionless parameters are being introduced.

$$\mathcal{Y}=\frac{\bar{T}}{\bar{T}_b},\quad \mathcal{Y}_a=\frac{\bar{T}_a}{\bar{T}_b},\quad \mathcal{Y}_s=\frac{\bar{T}_s}{\bar{T}_b},\quad \xi=\frac{\bar{x}}{L},\quad C=\frac{\tilde{\delta}}{t_b},\quad B=\tilde{\beta}T_b,\quad N_c=\frac{2\rho_{fg}\tilde{\beta}_f C_p K\bar{T}_b L^2}{v_f t_b K_{eff}},$$
$$N_r=\frac{2\eta_s\sigma\bar{T}_b^3L^2}{t_bK_{eff}},\quad m_0=\frac{2h_aL^2(1-\tilde{\phi})}{t_bK_{eff}},\quad m_1=\frac{2h_a i_{fg}L^2b_2(1-\tilde{\phi})}{t_bK_{eff}C_p\tilde{L}e^{\frac{2}{3}}},\quad G=\frac{\tilde{q}_a^*L^2}{\bar{T}_bK_{eff}},$$
$$m_2=m_1+m_0,(\tilde{w}-\tilde{w}_a)=b_2(\bar{T}-\bar{T}_a),\ \eta_G=\eta_g\bar{T}_b\,, \tag{14}$$

Where $\mathcal{Y}_a$ and $\mathcal{Y}_r$ are sink temperature and ambient temperature, C is taper's fin ratio, η_G is a dimensionless internal heat generation parameter, and G is a generation parameter. Also, N_c, N_r are radiative and convective heat coefficients and m_2 is the porous wet parameter. Eq. (12) may be expressed as follows in non-dimensionless terms:

$$(1-C\xi)\frac{d^2\mathcal{Y}(\xi)}{d\xi^2}-C\frac{d\mathcal{Y}(\xi)}{d\xi}+G(1-C\xi)+G\eta_G(\mathcal{Y}(\xi)-\mathcal{Y}_a)(1-C\xi)-m_2\frac{(\mathcal{Y}(\xi)-\mathcal{Y}_a)^{m+1}}{(1-\mathcal{Y}_a)^m}$$
$$-N_c(\mathcal{Y}(\xi)-\mathcal{Y}_a)^2\sin\varepsilon-N_r(\mathcal{Y}^4(\xi)-\mathcal{Y}_s^4)-N_rB\big(\mathcal{Y}(\xi)-\mathcal{Y}_s(\xi)\big)(\mathcal{Y}^4(\xi)-\mathcal{Y}_s^4)=0, \tag{15}$$

Subjected to initial and boundary conditions

$$\mathcal{Y}(0) = 0 \quad \text{and} \quad \frac{d\mathcal{Y}(1)}{d\xi} = 0, \tag{16}$$

Where the longitudinal fin's profiles are represented by

i. $C < 0$ is dovetail profile.
ii. $0 < C < 1$ is trapezoidal profile.
iii. $C = 0$ is rectangular profile.

At the fin base, the fin rate of heat transfer is expressed as

$$\tilde{q}_{\bar{x}} = -K_{eff} A_b \frac{d\bar{T}(0)}{d\bar{x}}, \tag{17}$$

The fin's base is in the area A_b. The fin's heat transfer rate is expressed in dimensionless form as

$$Q = \frac{\tilde{q}\, L}{K_{eff} A_b \bar{T}_b} = -\frac{d\mathcal{Y}(0)}{d\xi}. \tag{18}$$

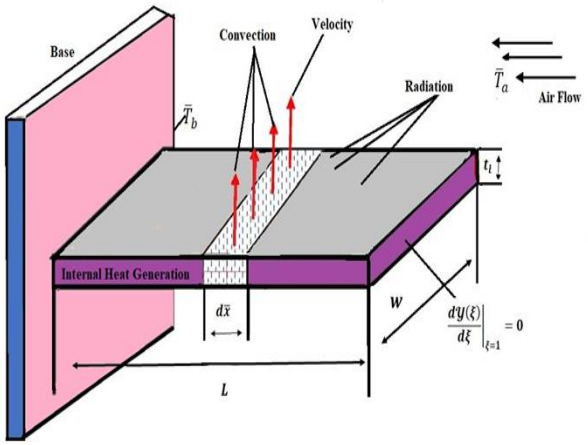

Fig. 1. Heat transfer modes and porous fin structure

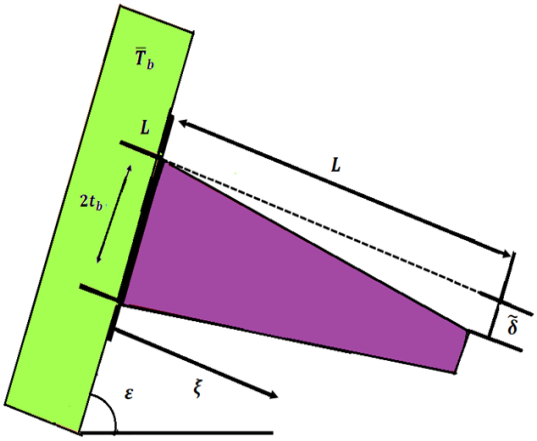

Fig. 2. Inclined longitudinal fin

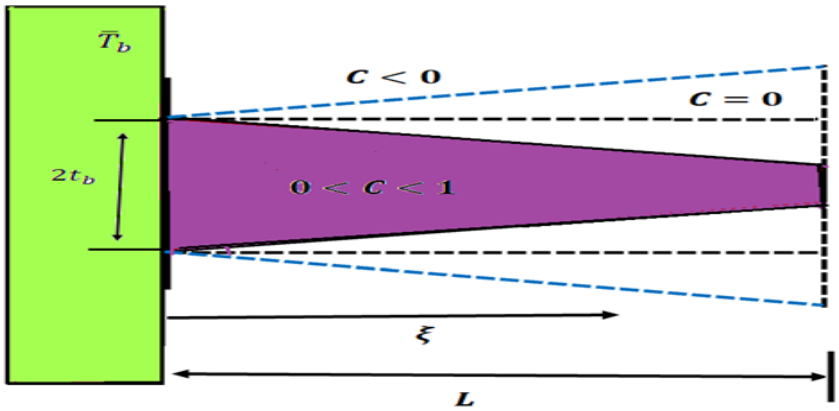

Fig. 3. Various profiles of the fin based on the values of fin taper ratio C

2.1 The Ideal Basic of Optimal Differential Transform Method

The differential transformation technique was developed by Zhou in 1986. This approach was developed to solve non-linear initial value problems. To construct idea the differential transformation technique, we can be defined the ordinary differential equation as follows:

$$\mathcal{L}[\mathcal{Y}(\xi)] + \mathbb{N}[\mathcal{Y}(\xi)] - \mathcal{F}(\xi) = 0, \tag{19}$$

Where ξ denotes an independent variable, $\mathcal{Y}(\xi)$ is unknown function and $\mathcal{F}(\xi)$ is known function. $\mathcal{L}$ and $\mathbb{N}$ are boundary linear and nonlinear operators. The following basic definitions and optimal differential transformation procedures are introduced for the function (ξ) :

$$\mathcal{W}(k) = \frac{1}{\bar{k}!}\left(\frac{d^{\bar{k}}\mathcal{Y}(\xi)}{d\xi^{\bar{k}}}\right)_{\xi=\xi_0}, \tag{20}$$

Now, can be noticed $\mathcal{Y}(\xi)$ is the original function which stated in practical applications as infinite series and $\mathcal{W}(k)$ is the transformed function. The inverse transform of the function $\mathcal{W}(k)$ can be expressed as follows:

$$\mathcal{Y}(\xi) = \sum_{k=0}^{\infty} \mathcal{W}(k)(\xi - \xi_0)^{\bar{k}}, \tag{21}$$

Substituting Eq. (20) and Eq. (21) into Eq. (19), yield

$$\mathcal{L}[\ \sum_{\bar{k}=0}^{\infty} \frac{(\xi-\xi_0)^{\bar{k}}}{\bar{k}!}\left(\frac{d^{\bar{k}}\mathcal{Y}(\xi)}{d\xi^{\bar{k}}}\right)_{\xi=\xi_0}] + \mathbb{N}[\ \sum_{\bar{k}=0}^{\infty} \frac{(\xi-\xi_0)^{\bar{k}}}{\bar{k}!}\left(\frac{d^{\bar{k}}\mathcal{Y}(\xi)}{d\xi^{\bar{k}}}\right)_{\xi=\xi_0}] - \mathcal{F}(\xi) = 0 \tag{22}$$

Consequently, can be reassigned the optimal coefficients Π_k, $k = 0,1,2,\dots,n$ in obtained series solution in Eq. (22) to get the residual function:

$$\mathcal{R}(\xi, \Pi_0,\ \Pi_1,\ \Pi_2, \dots, \Pi_n) = \mathcal{L}[\mathcal{Y}(\xi; \Pi_0, \Pi_1, \Pi_2, \dots, \Pi_n)] + \mathbb{N}[\mathcal{Y}(\xi; \Pi_0, \Pi_1, \Pi_2, \dots, \Pi_n)] - \mathcal{F}(\xi),$$

An approximate analytical solution can be defined by the presence of optimal coefficients as follows:

$$\mathcal{Y}(\xi; \Pi_0, \Pi_1, \Pi_2, \dots, \Pi_n) = \sum_{\bar{k}=0}^{\infty} \Pi_k \frac{(\xi-\xi_0)^{\bar{k}}}{\bar{k}!}\left(\frac{d^{\bar{k}}\mathcal{Y}(\xi)}{d\xi^{\bar{k}}}\right)_{\xi=\xi_0}, \tag{23}$$

There are several methods to determine the optimal values for Π_k, $k = 0,1,2,..,n$. Now, we implement the least squares method [29] and Galerkin method [30] to obtain the best coefficients for ξ can be described below:

i. The least square method

$$\mathcal{H}(\xi, \Pi_0, \Pi_1, \dots, \Pi_n) = \int_0^1 \mathcal{R}^2(\xi, \Pi_0, \Pi_1, \dots, \Pi_n)d\xi, \tag{24}$$

To find the value of minimizing $\mathcal{H}(\xi, \Pi_0, \Pi_1, \dots, \Pi_n)$ by using $\frac{\partial \mathcal{H}}{\partial \Pi_k} = 0,\ k = 0,1,2,..,n.$

ii.The Galerkin method

$$\int_a^b \mathcal{R}(\xi, \Pi_0, \Pi_1, \dots, \Pi_n)\ \frac{\partial \tilde{\mathcal{Y}}(\xi)}{\partial \Pi_k} d\xi = 0, \tag{25}$$

To find approximate value of $\Pi_k,\ k = 0,1,2,..,n$, we need the values of a and b can be from the domain of the ordinary differential equation. The fundamental, often employed differential transform mathematical operations are derived and are given in Table 1 as follows:

Table 1
The functions of differential transformation

	Original function	Transformed function
1	$\mathcal{Y}(\xi) = t(\xi) \pm v(\xi)$	$\mathcal{W}(k) = T(k) \pm V(k)$
2	$\mathcal{Y}(\xi) = \epsilon t(\xi)$	$\mathcal{W}(k) = \epsilon\ T(k)$, ϵ is constant
3	$\mathcal{Y}(\xi) = t(\xi)v(\xi)$	$\mathcal{W}(k) = \sum_{i=0}^{\bar{k}} T(i)V(k-i)$
4	$\mathcal{Y}(\xi) = \frac{d^n t(\xi)}{d\xi^n}$	$\mathcal{W}(k) = \frac{(k+n)!}{k!} T(k+n)$

2.2 The Application of Optimal Differential Transform Method and BVP4c

In this part, the optimal differential transform method and BVP4c are both used to resolve thermal profiles and Heat transfer in an inclined longitudinal porous fin. These are approximate analytical and numerical solutions, which may be summarized up as follows:

i. Analytical aspect

The construct of the iterative approach for Eq. (15) provided below using Table 1 of the differential transform technique in two cases first $m = 0$ as follows:

$$\begin{aligned}
&\left(\bar{k}+1\right)\left(\bar{k}+2\right)\mathcal{W}\left(\bar{k}+2\right) - \mathrm{C}\sum_{i=0}^{\bar{k}} \delta(\mathrm{i}-1)\left(\bar{k}-\mathrm{i}+1\right)\left(\bar{k}-\mathrm{i}+2\right)\mathcal{W}\left(\bar{k}-\mathrm{i}+2\right) - \\
&\mathrm{C}\left(\bar{k}+1\right)\mathcal{W}\left(\bar{k}+1\right) + (\mathrm{G} - \mathrm{G}\mathcal{Y}_a - N_c \sin(\varepsilon)\mathcal{Y}_a^2 + N_r\mathcal{Y}_s^4 - N_r \mathrm{B}\mathcal{Y}_s^5)\delta\left(\bar{k}\right) + (\eta_G \mathrm{CG}\mathcal{Y}_a - \mathrm{CG}) \\
&\delta\left(\bar{k}-1\right) + (\eta_G \mathrm{G} + 2N_c \sin(\varepsilon)\mathcal{Y}_a + N_r \mathrm{B}\mathcal{Y}_s^4) - \eta_G\ \mathrm{CG}\sum_{i=0}^{\bar{k}} \delta(\mathrm{i}-1)\mathcal{W}\left(\bar{k}-\mathrm{i}\right) + (\mathrm{B}N_r\mathcal{Y}_s - N_r) \\
&N_r \mathrm{B}\sum_{j=0}^{\bar{k}}\sum_{i=0}^{\bar{k}-j}\sum_{\bar{s}=0}^{\bar{k}-\mathrm{i}-\mathrm{j}}\sum_{l=0}^{\bar{k}-\mathrm{i}-\mathrm{j}-\bar{s}} \mathcal{W}(\mathrm{j})\,\mathcal{W}\left(\bar{k}-\mathrm{j}\right)\mathcal{W}\left(\bar{k}-\mathrm{i}-\mathrm{j}\right)\mathcal{W}\left(\bar{k}-\mathrm{i}-\mathrm{j}-\bar{\mathrm{s}}\right) - N_c \sin(\varepsilon) \\
&-\sum_{i=0}^{\bar{k}} \mathcal{W}(\mathrm{i})\mathcal{W}\left(\bar{k}-\mathrm{i}\right) - m_2\left(\mathcal{W}\left(\bar{k}\right) - \mathcal{Y}_a\delta\left(\bar{k}\right)\right)
\end{aligned} \tag{26}$$

The boundary conditions can be written as follows:

$$\mathcal{W}(0) = \Pi_0\ ,\ \mathcal{W}(1) = \Pi_1 \tag{27}$$

Where $\Pi_0 = \mathcal{Y}(0)$ and $\frac{d\mathcal{Y}(0)}{d\xi} = \Pi_1$. The value of Π_1 is unknown can be determined using $\mathcal{Y}(1) = 0$ and using the iterative solution of Eq. (15) and Eq. (16) and we get approximant analytical solutions for $\mathcal{Y}$:

$$\mathcal{Y}_1(\xi) = 1 + \Pi_1\xi,$$
$$\mathcal{Y}_2(\xi) = 1 + \Pi_1\xi + \frac{1}{2}(N_r(\mathrm{B}\mathcal{Y}_s^5 - \mathrm{B}\mathcal{Y}_s^4 - \mathcal{Y}_s^4 - \mathrm{B}\mathcal{Y}_s + 1) + \sin(\varepsilon)\, N_c(\mathcal{Y}_a^2 - 2\mathcal{Y}_a + 1) + \mathrm{G}\,\eta_G\,(\mathcal{Y}_a - 1) + \mathcal{Y}_s\mathrm{B} + \mathrm{C}\Pi_1) + m_2(1 - \mathcal{Y}_a))\xi^2$$
$$\mathcal{Y}_3(\xi) = 1 + \Pi_1\xi + \tfrac{1}{2}(N_r(\mathrm{B}\mathcal{Y}_s^5 - \mathrm{B}\mathcal{Y}_s^4 - \mathcal{Y}_s^4 - \mathrm{B}\mathcal{Y}_s + 1) + \sin(\varepsilon)\, N_c(\mathcal{Y}_a^2 - 2\mathcal{Y}_a + 1) + \mathrm{G}\,\eta_G\,(\mathcal{Y}_a - 1) + \mathcal{Y}_s\mathrm{B} + \mathrm{C}\Pi_1) + m_2(1 - \mathcal{Y}_a))\xi^2 + \tfrac{1}{6}\big(N_c\sin(\varepsilon)\,(2\mathrm{a}(1 - \mathcal{Y}_a) + 2\mathrm{C}(1 - 2\mathcal{Y}_a + \mathcal{Y}_a^2)) + N_r(B\mathrm{a}(2 + \Pi_1 + \Pi_1^2 + \Pi_1^3) + 2\mathrm{C}(\mathrm{B} - \mathcal{Y}_s^4 + 1) + \Pi_1(2 + \Pi_1 + \Pi_1^2) - \Pi_1\mathrm{B}\mathcal{Y}_s(\Pi_1 - 1 - \mathcal{Y}_s^3 - \Pi_1^2) - 2\mathrm{CB}\mathcal{Y}_s(\mathcal{Y}_s^3 - 1 + \mathcal{Y}_s^4)) + \mathrm{G}\eta_G(\mathrm{C}\mathcal{Y}_a - \Pi_1 - \mathrm{C}) + m_2(\Pi_1 - 4\mathrm{C}\mathcal{Y}_a + 2\mathrm{C}) + \mathrm{C}(2\Pi_1\mathrm{C} - \mathrm{G}))\xi^2.$$

The required approximate analytical solution of $\mathcal{Y}(\xi)$ is

$$\mathcal{Y}(\xi) = 1 + \Pi_1\xi + \tfrac{1}{2}(N_r(\mathrm{B}\mathcal{Y}_s^5 - \mathrm{B}\mathcal{Y}_s^4 - \mathcal{Y}_s^4 - \mathrm{B}\mathcal{Y}_s + 1) + \sin(\varepsilon)\, N_c(\mathcal{Y}_a^2 - 2\mathcal{Y}_a + 1) + \mathrm{G}\,\eta_G\,(\mathcal{Y}_a - 1) + \mathcal{Y}_s\mathrm{B} + \mathrm{C}\Pi_1) + m_2(1 - \mathcal{Y}_a))\xi^2 + \tfrac{1}{6}\big(N_c\sin(\varepsilon)\,(2\mathrm{a}(1 - \mathcal{Y}_a) + 2\mathrm{C}(1 - 2\mathcal{Y}_a + \mathcal{Y}_a^2)) + N_r(B\mathrm{a}(2 + \Pi_1 + \Pi^2 + \Pi^3) + 2\mathrm{C}(\mathrm{B} - \mathcal{Y}_s^4 + 1) + \Pi_1(2 + \Pi_1 + \Pi^2) - \Pi_1\mathrm{B}\mathcal{Y}_s(\Pi_1 - 1 - \mathcal{Y}_s^3 - \Pi^2) - 2\mathrm{CB}\mathcal{Y}_s(\mathcal{Y}_s^3 - 1 + \mathcal{Y}_s^4)) + \mathrm{G}\eta_G(\mathrm{C}\mathcal{Y}_a - \Pi_1 - \mathrm{C}) + m_2(\Pi_1 - 4\mathrm{C}\mathcal{Y}_a + 2\mathrm{C}) + \mathrm{C}(2\mathrm{Ca} - \mathrm{G}))\xi^2 + \tag{28}$$

The second case is $m = 1$, yield

$$\begin{aligned}
&(\bar{k} + 1)(\bar{k} + 2)\mathcal{W}(\bar{k} + 2) - \mathrm{C}\textstyle\sum_{i=0}^{\bar{k}}\delta(\mathrm{i} - 1)(\bar{k} - \mathrm{i} + 1)(\bar{k} - \mathrm{i} + 2)\mathcal{W}(\bar{k} - \mathrm{i} + 2) - \\
&\mathrm{C}(\bar{k} + 1)\mathcal{W}(\bar{k} + 1) + (\mathrm{G} - \mathrm{G}\mathcal{Y}_a - N_c\sin(\varepsilon)\mathcal{Y}_a^2 + N_r\mathcal{Y}_s^4 - N_r\mathrm{B}\mathcal{Y}_s^5)\delta(\bar{k}) + (\eta_G\mathrm{CG}\mathcal{Y}_a - \mathrm{CG})\delta(\bar{k} - 1) \\
&(\mathrm{G} - \mathrm{G}\mathcal{Y}_a - N_c\sin(\varepsilon)\mathcal{Y}_a^2 + N_r\mathcal{Y}_s^4 - N_r\mathrm{B}\mathcal{Y}_s^5)\delta(\bar{k}) + (\eta_G\mathrm{CG}\mathcal{Y}_a - \mathrm{CG})\delta(\bar{k} - 1) + (\eta_G\mathrm{G} + 2N_c\sin(\varepsilon)\mathcal{Y}_a \\
&+N_r\mathrm{B}\mathcal{Y}_s^4 - \eta_G\,\mathrm{CG}\sum_{i=0}^{\bar{k}}\delta(\mathrm{i} - 1)\mathcal{W}(\bar{k} - \mathrm{i}) + (\mathrm{B}N_r\mathcal{Y}_s - N_r)\left(\sum_{j=0}^{\bar{k}}\sum_{i=0}^{\bar{k}-j}\sum_{s=0}^{\bar{k}-\mathrm{i}-\mathrm{j}}\mathcal{W}(\mathrm{j})\mathcal{W}(\bar{k} - \mathrm{j})\mathcal{W}(\bar{k} - \mathrm{i} - \mathrm{j})\right. \\
&\left.\mathcal{W}(\bar{k} - \mathrm{i} - \mathrm{j} - \bar{\mathrm{s}})\right) - N_r\mathrm{B}\sum_{j=0}^{\bar{k}}\sum_{i=0}^{\bar{k}-j}\sum_{\bar{\mathrm{s}}=0}^{\bar{k}-\mathrm{i}-\mathrm{j}}\sum_{l=0}^{\bar{k}-\mathrm{i}-\mathrm{j}-\bar{\mathrm{s}}}\mathcal{W}(\mathrm{j})\mathcal{W}(\bar{k} - \mathrm{j})\mathcal{W}(\bar{k} - \mathrm{i} - \mathrm{j})\mathcal{W}(\bar{k} - \mathrm{i} - \mathrm{j} - \bar{\mathrm{s}}) \\
&\mathcal{W}(\bar{k} - \mathrm{i} - \bar{\mathrm{s}} - \mathrm{l}) - N_c\sin(\varepsilon)\sum_{i=0}^{\bar{k}}\mathcal{W}(\mathrm{i})\mathcal{W}(\bar{k} - \mathrm{i}) \\
&- \frac{m_2}{1 - \mathcal{Y}_a}\left(\sum_{j=0}^{\bar{k}}\mathcal{W}(\mathrm{j})\mathcal{W}(\bar{k} - \mathrm{j}) - 2\mathcal{Y}_a\mathcal{W}(\bar{k}) + \mathcal{Y}_a^2\delta(\bar{k})\right)
\end{aligned} \tag{29}$$

The iterative approximate analytical solutions of Eq. (15) and Eq. (16) for $\mathcal{Y}$ is

$$\mathcal{Y}_1(\xi) = 1 + \Pi_1\xi$$
$$\mathcal{Y}_2(\xi) = 1 + \Pi_1\xi + \frac{1}{2}(N_rB\mathcal{Y}_s(\mathcal{Y}_s^4 - \mathcal{Y}_s^3 - 1) - N_rB(\mathcal{Y}_s^4 + 1) + N_c\sin(\varepsilon)\,(\mathcal{Y}_a^2 - 2\mathcal{Y}_a + 1) + G(\eta_G\mathcal{Y}_a - \eta_G - 1) + m_2(1 - \mathcal{Y}_a) + C\Pi + N_r)\xi^2$$
$$\mathcal{Y}_3(\xi) = 1 + \Pi_1\xi + \frac{1}{2}(N_rB\mathcal{Y}_s(\mathcal{Y}_s^4 - \mathcal{Y}_s^3 - 1) - N_rB(\mathcal{Y}_s^4 + 1) + N_c\sin(\varepsilon)\,(\mathcal{Y}_a^2 - 2\mathcal{Y}_a + 1) + G(\eta_G\mathcal{Y}_a - \eta_G - 1) + m_2(1 - \mathcal{Y}_a) + C\Pi + N_r)\xi^2 + \frac{1}{6}\big(N_c\sin(\varepsilon)\big(2\Pi_1 + 2C - 2\Pi\mathcal{Y}_a + 2C\mathcal{Y}_s^2 - 4C\mathcal{Y}_a\big) + \mathrm{B}N_r(2\mathrm{C} + 2\Pi_1 + \Pi^2 + \Pi^3 + \Pi^4 + 2C\mathcal{Y}_s^5) + + \mathrm{B}N_r\mathcal{Y}_s\big(2\Pi_1 - \Pi^2 - 2C - C\mathcal{Y}_s^3 - \Pi_1\mathcal{Y}_s^3 - \Pi^3\big) + N_r(2C - 2C\mathcal{Y}_s^2 + 2\Pi_1 + \Pi_1^2 + \Pi_1^3 + 2C) + \mathrm{CG}(\eta_G\mathcal{Y}_a - \eta_G - 1) + m_2(2\Pi_1 + 2\mathrm{C} - 2C\mathcal{Y}_a) + 2\mathrm{C}^2\Pi_1 - 2\Pi_1\mathrm{G})\xi^3$$

The required approximate analytical solution of $\mathcal{Y}(\xi)$ is,

$$\mathcal{Y}(\xi) = 1 + \Pi_1\xi + \frac{1}{2}(N_r B\mathcal{Y}_s(\mathcal{Y}_s^4 - \mathcal{Y}_s^3 - 1) - N_r B(\mathcal{Y}_s^4 + 1) + N_c \sin(\varepsilon)(\mathcal{Y}_a^2 - 2\mathcal{Y}_a + 1)$$
$$+ G(\eta_G\mathcal{Y}_a - \eta_G - 1) + m_2(1 - \mathcal{Y}_a) + C\Pi + N_r)\xi^2 + \frac{1}{6}\left(N_c\sin(\varepsilon)\left(2\Pi_1 + 2C - 2\Pi\mathcal{Y}_a + 2C\mathcal{Y}_s^2 - 4C\mathcal{Y}_a\right)\right.$$
$$+\mathrm{B}N_r(2\mathrm{C} + 2\Pi_1 + \Pi^2 + \Pi^3 + \Pi^4 + 2C\mathcal{Y}_s^5) + +\mathrm{B}N_r\mathcal{Y}_s\left(2\Pi_1 - \Pi^2 - 2C - C\mathcal{Y}_s^3 - \Pi_1\mathcal{Y}_s^3 - \Pi^3\right) + N_r$$
$$(2C - 2C\mathcal{Y}_s^2 + 2\Pi_1 + \Pi_1^3 + 2C) + \mathrm{CG}(\eta_G\mathcal{Y}_a - \eta_G - 1) + m_2(2\Pi_1 + 2\mathrm{C} - 2C\mathcal{Y}_a) + 2\mathrm{C}^2\Pi_1 - 2\Pi_1\mathrm{G})\xi^3 + \qquad (30)$$

ii. Improve analytical aspect

For the purpose of improving the approximate analytical solution obtained from DTM in Eq. (28) and Eq. (30) which includes $\xi, \xi^2, \xi^3, \xi^4, \xi^5, \xi^6$, we assume the approximate analytical solution in the following form:

$$\tilde{\mathcal{Y}}(\xi) = \Pi_0 + \Pi_1\xi + \Pi_2\xi^2 + \Pi_3\xi^3 + \Pi_4\xi^4 + \Pi_5\xi^5 + \Pi_6\xi^6\,, \qquad (31)$$

The equation for the residual can be obtained by substituting Eq. (31) into Eq. (15), we have

$$\mathcal{R}(\Pi_0, \dots, \Pi_6) = (-\mathrm{C}\xi + 1)(2\Pi_2 + 6\Pi_3\xi + 12\Pi_4\xi^2 + 20\Pi_5\xi^3 + 30\Pi_6\xi^4) - C(\Pi_1 + 2\Pi_2\xi + 3\Pi_3\xi^2 + 4\Pi_4\xi^3 + 5\Pi_5\xi^4$$
$$+6\Pi_6\xi^5) + 5\Pi_5\xi^4 + 6\Pi_6\xi^5) + G\left(1 + \eta_G\left(\left(\Pi_0 + \Pi_1\xi + \Pi_2\xi^2 + \Pi_3\xi^3 + \Pi_4\xi^4 + \Pi_5\xi^5 + \Pi_6\xi^6\right) - \mathcal{Y}_a\right)(1 - C\xi)\right.$$
$$+\frac{m_2}{(1-\mathcal{Y}_a)^m}\left((\Pi_0 + \Pi_1\xi + \Pi_2\xi^2 + \Pi_3\xi^3 + \Pi_4\xi^4 + \Pi_5\xi^5 + \Pi_6\xi^6) - \mathcal{Y}_a\right)^{m+1} - N_c(\Pi_0 + \Pi_1\xi + \Pi_2\xi^2 +$$
$$\Pi_3\xi^3 + \Pi_4\xi^4 + \Pi_5\xi^5 + \Pi_6\xi^6) + \mathcal{Y}_a)^2\sin\varepsilon + N_r\left(1 + B\left((\Pi_0 + \Pi_1\xi + \Pi_2\xi^2 + \Pi_3\xi^3 + \Pi_4\xi^4 + \Pi_5\xi^5 + \Pi_6\xi^6\right)\right.$$
$$-\mathcal{Y}_r)(\Pi_0 + \Pi_1\xi + \Pi_2\xi^2 + \Pi_3\xi^3 + \Pi_4\xi^4 + \Pi_5\xi^5 + \Pi_6\xi^6)^4 - \mathcal{Y}_s^4) + \Pi_4\xi^4 + \Pi_5\xi^5 + \Pi_6\xi^6)^4 - \mathcal{Y}_s^4) \qquad (32)$$

To determine the appropriate values for $\Pi_k, k = 0,1,2,4,5,6$. We employ the least squares optimizer to get the best coefficients for ξ when boundary conditions in Eq. (16) are used. The steps are described by the following:

$$\Pi_0 = 1, \qquad (33\text{-a})$$

$$\Pi_1 = -(2\Pi_2 + 3\Pi_3 + 4\Pi_4 + 5\Pi_5 + 6\Pi_6), \qquad (33\text{-b})$$

Substituting Eq. (33) in Eq. (31), we get

$$\tilde{\mathcal{Y}}(\xi) = 1 - (2\Pi_2 + 3\Pi_3 + 4\Pi_4 + 5\Pi_5 + 6\Pi_6)\xi + \Pi_2\xi^2 + \Pi_3\xi^3 + \Pi_4\xi^4 + \Pi_5\xi^5 + \Pi_6\xi^6\,. \qquad (34)$$

The next residual function $\mathcal{R}(\xi, \Pi_0, \Pi_1, \Pi_2, \Pi_3, \Pi_4.\Pi_5, \Pi_6)$ will be produced when it is compensated Eq. (34) into Eq. (15), yield

$$\mathcal{R}(\xi, \Pi_2, \Pi_3, \Pi_4.\Pi_5, \Pi_6) = (-\mathrm{C}\xi + 1)(2\Pi_2 + 6\Pi_3\xi + 12\Pi_4\xi^2 + 20\Pi_5\xi^3 + 30\Pi_6\xi^4) -$$
$$-C(-(2\Pi_2 + 3\Pi_3 + 4\Pi_4 + 5\Pi_5 + 6\Pi_6) + 2\Pi_2\xi + 3\Pi_3\xi^2 + 4\Pi_4\xi^3 + 5\Pi_5\xi^4 + 6\Pi_6\xi^5) + G(1 +$$
$$\eta_G\left((1 - (2\Pi_2 + 3\Pi_3 + 4\Pi_4 + 5\Pi_5 + 6\Pi_6)\xi + \Pi_2\xi^2 + \Pi_3\xi^3 + \Pi_4\xi^4 + \Pi_5\xi^5 + \Pi_6\xi^6) - \mathcal{Y}_a\right)(1 - C\xi)$$
$$+\frac{m_2}{(1-\mathcal{Y}_a)^m}\left((1 - (2\Pi_2 + 3\Pi_3 + 4\Pi_4 + 5\Pi_5 + 6\Pi_6)\xi + \Pi_2\xi^2 + \Pi_3\xi^3 + \Pi_4\xi^4 + \Pi_5\xi^5 + \Pi_6\xi^6) - \mathcal{Y}_a\right)^{m+1}$$
$$-N_c\left((1 - (2\Pi_2 + 3\Pi_3 + 4\Pi_4 + 5\Pi_5 + 6\Pi_6)\xi + \Pi_2\xi^2 + \Pi_3\xi^3 + \Pi_4\xi^4 + \Pi_5\xi^5 + \Pi_6\xi^6) + \mathcal{Y}_a\right)^2\sin\varepsilon$$
$$N_r\left(1 + B\left((1 - (2\Pi_2 + 3\Pi_3 + 4\Pi_4 + 5\Pi_5 + 6\Pi_6)\xi + \Pi_2\xi^2 + \Pi_3\xi^3 + \Pi_4\xi^4 + \Pi_5\xi^5 + \Pi_6\xi^6) - \mathcal{Y}_r\right)\right.$$
$$((1 - (2\Pi_2 + 3\Pi_3 + 4\Pi_4 + 5\Pi_5 + 6\Pi_6)\xi + \Pi_2\xi^2 + \Pi_3\xi^3 + \Pi_4\xi^4 + \Pi_5\xi^5 + \Pi_6\xi^6)^4 - \mathcal{Y}_s^4). \qquad (35)$$

It is possible to determine the best values for Π_k from $\frac{\partial \mathcal{H}}{\partial \Pi_k} = 0$, after calculating

$\mathcal{H}(\xi, \Pi_2, \Pi_3, \Pi_4, \Pi_5, \Pi_6) = \int_0^1 \mathcal{R}^2(\xi, \Pi_2, \Pi_3, \Pi_4, \Pi_5, \Pi_6) d\xi.$

Finding the values of all the coefficients, we will substitute them into its Eq. (31), thus finding the approximate analytical solution. In the Galerkin method to obtain the optimal coefficients for ξ by using Eq. (35), we can find every coefficient by solve the following system for Π_k for each $\mathrm{k} = 2,3,4,5,6$.

$$\int_0^1 \mathcal{R}(\xi, \Pi_2, \Pi_3, \Pi_4. \Pi_5, \Pi_6) \frac{\partial \tilde{\mathcal{Y}}(\xi)}{\partial \Pi_i} d\xi = 0 \quad (36)$$

iii. Numerical aspect

The bvp4c solver in MATLAB is used to solve Eq. (15) which is a nonlinear ordinary differential equation subject to initial and boundary conditions Eq. (16). The solution is a fourth order precision finite difference code. Applying the solution requires rewriting the equation as a set of equivalent first order ordinary differential equations, become

$$\mathcal{Y}(\xi) = \mathcal{F}_1 , \ \frac{d\mathcal{Y}(\xi)}{d\xi} = \mathcal{F}_2,$$
$$\frac{d\mathcal{F}_2}{d\xi} = \frac{-1}{(1-C\xi)}\left(C\mathcal{F}_2 + G(1-C\xi) + G\eta_G(\mathcal{F}_1 - \mathcal{Y}_1)(1-C\xi) - m_2 \frac{(\mathcal{F}_1 - \mathcal{Y}_1)^{m+1}}{(1-\mathcal{Y}_1)^m} \right)$$
$$- N_c(\mathcal{F}_1 - \mathcal{Y}_1)^2 \sin\varepsilon$$
$$-N_c(\mathcal{F}_1 - \mathcal{Y}_1)^2 \sin\varepsilon - N_r\left({\mathcal{F}_1}^4 - {\mathcal{Y}_2}^4\right) - N_r B(\mathcal{F}_1 - \mathcal{Y}_2) \quad (37)$$

From the boundary conditions Eq. (16), we obtain that

$$\mathcal{F}_1(0) = 1 , \ \mathcal{F}_1(1) = 0 \quad (38)$$

To establish an initial value problem, Eq. (37) and Eq. (38) have been numerically integrated to a predetermined end point. All these simplifications were necessary since the MATLAB package had to be utilized. The range from 0 to 1 and back is then resolved by running this program with a 0.1 step size.

iv. The analysis of the convergence test

In order to evaluate the errors of approximate analytical solutions to Eq. (15), we have applied the theorems [31, 32]. This theorem may be used to define the convergence condition, which is introduced as follows:

Definition 5.1: If there exists $0 \leq \pi_j < 1$ and for $j = 0,1,2, \ldots,$ then $\left\|\mathcal{W}_{j+1}\right\| \leq \pi_j \left\|\mathcal{W}_j\right\|$ is the condition of convergent. Tables 2-3 show that the convergence criterion is satisfied for all solutions as follows:

Table 2
The values of convergent for $\mathcal{Y}_a = 0.8$, $\mathcal{Y}_s = 0.8$, $G = 0.02, m_2 = 0.002, N_c = 1$, $N_r = 0.0001, \eta_G = 0.2$, $B = 0.2$ and $\varepsilon = \frac{\pi}{2}$

	$\boldsymbol{m=0}$			$\boldsymbol{m=1}$		
$\boldsymbol{\pi_j}$	$\boldsymbol{C=0}$	$\boldsymbol{C=0.1}$	$\boldsymbol{C=0.05}$	$\boldsymbol{C=0}$	$\boldsymbol{C=0.1}$	$\boldsymbol{C=0.05}$
$\boldsymbol{\pi_0}$	0.5635217698	0.5605491382	0.5620031453	0.5562702832	0.5531496157	0.554666424
$\boldsymbol{\pi_1}$	0.7529697065	0.7069627576	0.7300043538	0.7627853481	0.7170887036	0.739990997
$\boldsymbol{\pi_2}$	0.4167919801	0.3754622600	0.3957077300	0.4310934009	0.3901133436	0.410176802
$\boldsymbol{\pi_3}$	0.5261399781	0.5187061554	0.5210901835	0.5364805871	0.5275186915	0.530774904
$\boldsymbol{\pi_4}$	0.4359470258	0.3891779762	0.4131738167	0.4484873426	0.4025305179	0.426053214
$\boldsymbol{\pi_5}$	0.4557513128	0.4372697112	0.4447673434	0.4662160186	0.4465800081	0.454797909
⋮	⋮	⋮	⋮	⋮	⋮	⋮

Table 3
The values of convergent for $C = 0.1, \mathcal{Y}_a = 0.5$, $\mathcal{Y}_s = 0.1$, $G = 0.025, m_2 = 0.07, N_c = 1$, $N_r = 0.001, \eta_G = 0.2$, $B = 0.1$ and $\varepsilon = \frac{\pi}{2}$.

	$\boldsymbol{m=0}$			$\boldsymbol{m=1}$		
$\boldsymbol{\pi_j}$	$\boldsymbol{B=0}$	$\boldsymbol{B=0.1}$	$\boldsymbol{B=0.05}$	$\boldsymbol{B=0}$	$\boldsymbol{B=0.1}$	$\boldsymbol{B=0.05}$
$\boldsymbol{\pi_0}$	0.1142893506	0.1143609775	0.1143609775	0.1123416651	0.1124122875	0.1123769773
$\boldsymbol{\pi_1}$	0.5340433061	0.5340709579	0.5340709579	0.5441689590	0.5441959474	0.5441824524
$\boldsymbol{\pi_2}$	0.1027443383	0.1027935307	0.1027935307	0.1209041279	0.1209518491	0.1209279907
$\boldsymbol{\pi_3}$	0.4710286912	0.4709740493	0.4709740493	0.4545867883	0.4545635106	0.4545751376
$\boldsymbol{\pi_4}$	0.0979630358	0.09803973158	0.09803973158	0.1206099168	0.1206873781	0.1206486526
$\boldsymbol{\pi_5}$	0.4069108548	0.4067668298	0.4067668298	0.3769843722	0.3769006784	0.3769424964
⋮	⋮	⋮	⋮	⋮	⋮	⋮

3. Result

3.1 The Discussion of Tabular

In this section displays how inclined longitudinal porous fins of various profiles function in radiative and conductive settings when completely moisturized. The realization looks at the impact of changes in the emissivity parameter B, sink temperature $\mathcal{Y}_s$, power index m, ambient temperature $\mathcal{Y}_a$, coefficient of conductive parameter N_c, generation parameter G, wet porous parameter m_2, inclination angle ε, and coefficient of radiative parameter N_r on the temperature profiles $\mathcal{Y}(\xi)$. Tables 4-9 given a comparison of the findings of the DTM, LSDTM, and GDTM with the numerical outcome by the BVP4c for six cases are $(C = 0, m = 0)$, $(C = 0, m = 0)$, $(C = 0, m = 0)$, $(C = 0, m = 0)$, $(C = 0, m = 0)$, and $(C = 0, m = 0)$ respectively. From these tables explained that the LSDTM and GDTM given improvement of the heat profile of DTM by identifying the absolute errors. The Tables 10- 14 displayed convergence of value $\frac{d\mathcal{Y}(0)}{d\xi}$ which become the same in decimal places and remain constant when the iterative methods are increased further. The values of the heat transfer rate explained in Tables 15 -18 and these tables presented that the values of LSDTM and GDTM are more consistent with the numerical than DTM. The last table, which is a Table 19 displays from which the comparison of the resulting solutions of LSDTM with NARX-LM and CFB-LM. We can understand from this table gives that the resulting solutions of LSDTM have better results than NARX-LM and CFB-LMA.

Table 4
Comparison between BVP4c, DTM, LSDTM and GDTM for $C = 0$, $\mathcal{Y}_a = 0.8$, $\mathcal{Y}_s = 0.5$, $G = 0.02, m_2 = 0.002, N_c = 1, N_r = 0.00002, \eta_G = 0.2$, $B = 0.1, m = 0$ and $= \frac{\pi}{2}$

	Displayed Results				Absolute Errors		
ξ	BVP4	DTM	LSDTM	GDTM	$\boldsymbol{Error_{DTM}}$	$\boldsymbol{Error_{LSDTM}}$	$\boldsymbol{Error_{GDTM}}$
0.0	1.0000000	1.000000000	1.000000000	1.000000000	0000000000	0.00000000	0.00000000
0.1	0.99835638	0.998356362	0.998356384	0.998356384	2.40×10^{-8}	2.00×10^{-9}	2.00×10^{-9}
0.2	0.99690251	0.996902472	0.996902515	0.996902515	3.81×10^{-8}	5.01×10^{-9}	5.01×10^{-9}
0.3	0.99563267	0.995632609	0.995632672	0.995632672	6.12×10^{-8}	2.00×10^{-9}	2.00×10^{-9}
0.4	0.99454189	0.994541809	0.994541891	0.994541891	8.14×10^{-8}	1.00×10^{-9}	1.00×10^{-9}
0.5	0.99362593	0.993625836	0.993625935	0.993625935	9.46×10^{-8}	5.03×10^{-9}	5.03×10^{-9}
0.6	0.99288126	0.992881151	0.992881263	0.992881263	1.09×10^{-7}	3.02×10^{-9}	3.02×10^{-9}
0.7	0.99230501	0.992304888	0.992305012	0.992305012	1.22×10^{-7}	2.01×10^{-9}	2.01×10^{-9}
0.8	0.99189497	0.991894838	0.991894970	0.991894970	1.33×10^{-7}	0.00000000	0.00000000
0.9	0.99164957	0.991649432	0.991649569	0.991649569	1.39×10^{-7}	1.00×10^{-9}	3.02×10^{-9}

Table 5
Comparison between BVP4c, DTM, LSDTM and GDTM for $C = 0$, $\mathcal{Y}_a = 0.8$, $\mathcal{Y}_s = 0.5$, $G = 0.02, m_2 = 0.002, N_c = 1, N_r = 0.00002, \eta_G = 0.2$, $B = 0.1, m = 1$ and $\varepsilon = \frac{\pi}{2}$

ξ	Displayed Results				Absolute Errors		
	BVP4	DTM	LSDTM	GDTM	$\boldsymbol{Error_{DTM}}$	$\boldsymbol{Error_{LSDTM}}$	$\boldsymbol{Error_{GDTM}}$
0.0	1.000000000	1.000000000	1.00000000	1.00000000	000000000	1.0000000 0	0000000000
0.1	0.998357329	0.998357305	0.998357326	0.9983573269	2.40×10^{-8}	3.00×10^{-9}	2.10×10^{-9}
0.2	0.996904374	0.996904329	0.996904372	0.9969043727	4.51×10^{-8}	2.00×10^{-9}	1.30×10^{-9}
0.3	0.995635392	0.995635326	0.995635390	0.9956353904	6.62×10^{-8}	2.00×10^{-9}	1.60×10^{-9}
0.4	0.994545397	0.994545313	0.994545395	0.9945453956	8.44×10^{-8}	2.01×10^{-9}	1.40×10^{-9}
0.5	0.993630135	0.993630034	0.993630133	0.9936301331	1.01×10^{-7}	2.01×10^{-9}	1.91×10^{-9}
0.6	0.992886051	0.992885936	0.992886048	0.9928860488	1.15×10^{-7}	3.02×10^{-9}	2.21×10^{-9}
0.7	0.992310268	0.992310142	0.992310265	0.9923102656	1.26×10^{-7}	3.02×10^{-9}	2.41×10^{-9}
0.8	0.991900567	0.991900432	0.991900564	0.9919005647	1.41×10^{-7}	3.02×10^{-9}	2.31×10^{-9}
0.9	0.991655373	0.991655233	0.991655371	0.9916553710	1.44×10^{-7}	2.01×10^{-9}	2.01×10^{-9}
1.0	0.991573747	0.991573604	0.991573744	0.991573743	2.40×10^{-7}	3.02×10^{-9}	3.22×10^{-9}

Table 6
Comparison between BVP4c, DTM, LSDTM and GDTM for $C = 0.1, \mathcal{Y}_a = 0.8$, $\mathcal{Y}_s = 0.8$, $G = 0.02, m_2 = 0.002, N_c = 1, N_r = 0.00001, \eta_G = 0.2$, $B = 0.2, m = 0$ and $\varepsilon = \frac{\pi}{2}$

	Displayed Results				Absolute Errors		
ξ	BVP4	DTM	LSDTM	GDTM	$\boldsymbol{Error_{DTM}}$	$\boldsymbol{Error_{LSDTM}}$	$\boldsymbol{Error_{GDTM}}$
0.0	1.000000000	1.000000000	1.000000000	1.000000000	0.00000000	0.00000000	000000000
0.1	0.998264878	0.998264866	0.998264878	0.998264878	1.20×10^{-8}	0.00000000	0. 0000000
0.2	0.996706380	0.996706357	0.996706380	0.996706379	2.30×10^{-8}	0.00000000	1.00×10^{-9}
0.3	0.995323978	0.995323943	0.995323977	0.995323977	3.51×10^{-8}	1.00×10^{-9}	1.00×10^{-9}
0.4	0.994117884	0.994117839	0.994117883	0.994117883	4.52×10^{-8}	1.00×10^{-9}	1.00×10^{-9}
0.5	0.993089072	0.993089018	0.993089071	0.993089071	5.43×10^{-8}	1.00×10^{-9}	1.00×10^{-9}
0.6	0.992239296	0.992239234	0.992239295	0.992239295	6.24×10^{-8}	1.00×10^{-9}	1.00×10^{-9}
0.7	0.991571121	0.991571054	0.991571121	0.991571120	6.75×10^{-8}	0.00000000	1.00×10^{-9}
0.8	0.991087961	0.991087890	0.991087960	0.991087960	7.16×10^{-8}	1.00×10^{-9}	1.00×10^{-9}
0.9	0.990794120	0.990794045	0.990794118	0.990794118	7.56×10^{-8}	2.01×10^{-9}	2.01×10^{-9}
1.0	0.990694840	0.990694766	0.990694840	0.990694840	7.46×10^{-8}	0.00000000	0.00000000

Table 7
Comparison between BVP4c, DTM, LSDTM and GDTM for $C = 0.1, \mathcal{Y}_a = 0.8\,, \mathcal{Y}_s = 0.8\,, G = 0.02,$ $m_2 = 0.002, N_c = 1, N_r = 0.00001, \eta_G = 0.2\,, B = 0.2, m = 1$ and $\varepsilon = \frac{\pi}{2}$

	Displayed Results				Absolute Errors		
ξ	BVP4	DTM	LSDTM	GDTM	$\boldsymbol{Error_{DTM}}$	$\boldsymbol{Error_{LSDTM}}$	$\boldsymbol{Error_{GDTM}}$
0.0	1.000000000	1.000000000	1.00000000	1.000000000	0.00000000	0.00000000	0.00000000
0.1	0.998265902	0.998265890	0.998265902	0.998265902	1.29×10^{-8}	1.00×10^{-10}	1.00×10^{-10}
0.2	0.996708409	0.996708386	0.996708409	0.996708409	1.29×10^{-8}	8.02×10^{-10}	8.02×10^{-10}
0.3	0.995326964	0.995326929	0.995326962	0.995326963	3.56×10^{-8}	1.60×10^{-9}	1.50×10^{-9}
0.4	0.994121755	0.994121710	0.994121753	0.994121753	4.55×10^{-8}	1.71×10^{-9}	1.60×10^{-9}
0.5	0.993093733	0.993093679	0.993093731	0.993093732	5.46×10^{-8}	1.40×10^{-9}	1.30×10^{-9}
0.6	0.992244633	0.992244572	0.992244632	0.992244632	6.21×10^{-8}	9.07×10^{-10}	1.00×10^{-9}
0.7	0.991577005	0.991576938	0.991577004	0.991577004	6.80×10^{-8}	7.05×10^{-10}	1.10×10^{-9}
0.8	0.991094248	0.991094176	0.991094246	0.991094246	7.26×10^{-8}	1.31×10^{-9}	1.51×10^{-9}
0.9	0.990800653	0.990800579	0.990800651	0.990800651	7.53×10^{-8}	1.91×10^{-9}	1.81×10^{-9}
1.0	0.990701457	0.990701384	0.990701457	0.990701458	7.43×10^{-8}	1.00×10^{-10}	5.04×10^{-10}

Table 8
Comparison between BVP4c, DTM, LSDTM and GDTM for $C = -0.1, \mathcal{Y}_a = 0.9\,, \mathcal{Y}_s = 0.4\,, G = 0.01,$ $m_2 = 0.003, N_c = 1.5, N_r = 0.00002, \eta_G = 0.2\,, B = 0.1, m = 0$ and $\varepsilon = \frac{\pi}{2}$

	Displayed Results				Absolute Errors		
ξ	BVP4	DTM	LSDTM	GDTM	$\boldsymbol{Error_{DTM}}$	$\boldsymbol{Error_{LSDTM}}$	$\boldsymbol{Error_{GDTM}}$
0.0	1.000000000	1.000000000	1.000000000	1.00000000	000000000	0000000000	000000000
0.1	0.999605150	0.999605144	0.999605149	0.999605149	6.40×10^{-9}	9.00×10^{-10}	9.00×10^{-10}
0.2	0.999262482	0.999262470	0.999262481	0.999262481	1.13×10^{-8}	7.00×10^{-10}	7.00×10^{-10}
0.3	0.998968980	0.998968964	0.998968980	0.998968980	1.63×10^{-8}	6.00×10^{-10}	7.00×10^{-10}
0.4	0.998721863	0.998721843	0.998721863	0.998721863	2.09×10^{-8}	8.01×10^{-10}	8.01×10^{-10}
0.5	0.998518563	0.998518538	0.998518562	0.998518562	2.51×10^{-8}	1.00×10^{-9}	9.01×10^{-10}
0.6	0.998356708	0.998356680	0.998356707	0.998356707	2.86×10^{-8}	1.30×10^{-9}	1.20×10^{-9}
0.7	0.998234113	0.998234081	0.998234112	0.998234112	3.16×10^{-8}	1.40×10^{-9}	1.40×10^{-9}
0.8	0.998148760	0.998148727	0.998148759	0.998148759	3.36×10^{-8}	1.30×10^{-9}	1.40×10^{-9}
0.9	0.998098791	0.998098756	0.998098790	0.998098790	3.48×10^{-8}	1.10×10^{-9}	1.10×10^{-9}
1.0	0.998082492	0.998082456	0.998082491	0.998082491	3.57×10^{-8}	1.60×10^{-9}	1.60×10^{-9}

Table 9
Comparison between BVP4c, DTM, LSDTM and GDTM for $C = -0.1, \mathcal{Y}_a = 0.9\,, \mathcal{Y}_s = 0.4\,, G = 0.01,$ $m_2 = 0.003, N_c = 1.5, N_r = 0.00002, \eta_G = 0.2\,, B = 0.1, m = 1$ and $\varepsilon = \frac{\pi}{2}$

	Displayed Results				Absolute Errors		
ξ	BVP4	DTM	LSDTM	GDTM	$\boldsymbol{Error_{DTM}}$	$\boldsymbol{Error_{LSDTM}}$	$\boldsymbol{Error_{GDTM}}$
0.0	1.000000000	1.00000000	1.000000000	1.000000000	0.00000000	0.00000000	0.00000000
0.1	0.999605493	0.999605487	0.999605492	0.999605492	6.00×10^{-9}	1.00×10^{-9}	1.00×10^{-9}
0.2	0.999263153	0.999263142	0.999263153	0.999263153	1.10×10^{-8}	0.00000000	0.00000000
0.3	0.998969958	0.998969942	0.998969958	0.998969957	1.60×10^{-8}	0.00000000	1.00×10^{-9}
0.4	0.998723118	0.998723097	0.998723117	0.998723117	2.10×10^{-8}	1.00×10^{-9}	1.00×10^{-9}
0.5	0.998520059	0.998520034	0.998520058	0.998520058	2.50×10^{-8}	1.00×10^{-9}	1.00×10^{-9}
0.6	0.998358406	0.998358378	0.998358405	0.998358405	2.80×10^{-8}	1.00×10^{-9}	1.00×10^{-9}
0.7	0.998235971	0.998235939	0.998235969	0.998235969	3.20×10^{-8}	2.00×10^{-9}	2.00×10^{-9}
0.8	0.998150733	0.998150699	0.998150732	0.998150732	3.40×10^{-8}	1.00×10^{-9}	1.00×10^{-9}
0.9	0.998100832	0.998100797	0.998100831	0.998100831	3.50×10^{-8}	1.00×10^{-9}	1.00×10^{-9}
1.0	0.998084557	0.998084521	0.998084555	0.998084555	3.60×10^{-8}	2.00×10^{-9}	2.00×10^{-9}

Table 10

The convergent of $\frac{d\mathcal{Y}(0)}{d\xi}$ between BVP4c, DTM, LSDTM, and GDTM

	BVP4c		DTM		LSDTM		GDTM	
C	$m=0$	$m=1$	$m=0$	$m=1$	$m=0$	$m=1$	$m=0$	$m=1$
0.0	0.0084126	0.0080843	0.0084127	0.0080845	0.0084126	0.0080843	0.0084126	0.0080843
0.1	0.0079313	0.0076232	0.0079314	0.0076233	0.0079313	0.0076232	0.0079313	0.0076232
−0.1	0.0088947	0.0085467	0.0088948	0.0085469	0.0088947	0.0085467	0.0088947	0.0088947

Table 11

The convergent of $\frac{d\mathcal{Y}(0)}{d\xi}$ between BVP4c, DTM, LSDTM, and GDTM

	BVP4c		DTM		LSDTM		GDTM	
B	$m=0$	$m=1$	$m=0$	$m=1$	$m=0$	$m=1$	$m=0$	$m=1$
0.0	0.0083663	0.0080399	0.0083662	0.0080398	0.0083663	0.0080399	0.0083663	0.0080399
0.1	0.0083646	0.008038	0.0083644	0.008038	0.0083646	0.0080383	0.0083646	0.0080383
0.2	0.0083628	0.008036	0.0083627	0.008036	0.0083628	0.0080367	0.0083628	0.0080367

Table 12

The convergent of $\frac{d\mathcal{Y}(0)}{d\xi}$ between BVP4c, DTM, LDTM, and GDTM

	BVP4c		DTM		LSDTM		GDTM	
m_2	$m=0$	$m=1$	$m=0$	$m=1$	$m=0$	$m=1$	$m=0$	$m=1$
0.05	0.0089814	0.0087936	0.0089815	0.0087937	0.0089814	0.0087936	0.0089814	0.0087936
0.10	0.0083644	0.008038	0.0083645	0.0080383	0.0083644	0.008038	0.0083644	0.008038
2.00	-0.0063906	-0.005071	-0.0063907	-0.005141	-0.0063906	-0.005071	-0.0063906	-0.005071

Table 13

The convergent of $\frac{d\mathcal{Y}(0)}{d\xi}$ between BVP4c, DTM, LSDTM, and GDTM.

	BVP4c		DTM		LSDTM		GDTM	
G	$m=0$	$m=1$	$m=0$	$m=1$	$m=0$	$m=1$	$m=0$	$m=1$
0.01	0.0007549	0.0007544	0.000754	0.0007543	0.00075493	0.00075447	0.0007549	0.00075447
0.01	0.0095935	0.009584	0.0095933	0.009584	0.00959350	0.00958487	0.0095935	0.00958487
0.40	0.3702129	0.367220	0.370080	0.367051	0.37021297	0.36722059	0.3702129	0.36722059

Table 14

The convergence of values $\frac{d\mathcal{Y}(0)}{d\xi}$ for DTM when $\varepsilon=\frac{\pi}{2}$ and $\eta_G=0.2$

	$C=0, \mathcal{Y}_a=0.02, \mathcal{Y}_S=0.02, G=0.025$ $m_2=0.07, N_c=0.1, N_r=0.001,\ B=0.2$		$C=0.01, \mathcal{Y}_a=0.9, \mathcal{Y}_S=0.01, G=0.06$ $m_2=0.05, N_c=1, N_r=0.0001,\ B=0.1$	
Approximate Order	$m=0$	$m=1$	$m=0$	$m=1$
Order1	0.000000	0.000000	0.000000	0.000000
Order2	−0.135935	−0.135935	0.045633	0.045633
Order3	−0.120123	−0.116519	0.040953	0.040066
Order4	−0.125867	−0.123748	0.041994	0.041181
Order5	−0.125163	−0.122631	0.042337	0.041670
Order6	−0.125346	−0.122939	0.042238	0.041518
Order7	−0.125322	−0.122891	0.042255	0.041545
Order8	−0.125327	−0.122902	0.042253	0.041543
Order9	−0.125327	−0.122900	0.042253	0.041542
Order10	−0.125327	−0.122900	0.042253	0.041542

Table 15
The comparison of the values Q between BVP4c, DTM, LSDTM, and GDTM

	BVP4c		DTM		LSDTM		GDTM	
C	$m=0$	$m=1$	$m=0$	$m=1$	$m=0$	$m=1$	$m=0$	$m=1$
1.0	0.0015645	0.0015636	0.0015625	0.0015633	0.00156459	0.00156361	0.0015645	0.00156361
1.5	0.0027315	0.0027298	0.0027311	0.0027294	0.00273150	0.00272984	0.0027315	0.00272984
2.0	0.0034594	0.0038612	0.0038635	0.0038612	0.00345948	0.00386121	0.0034594	0.00386121

Table 16
The comparison of the values Q between BVP4c, DTM, LDTM, and GDTM

	BVP4c		DTM		LSDTM		GDTM	
N_r	$m=0$	$m=1$	$m=0$	$m=1$	$m=0$	$m=1$	$m=0$	$m=1$
0.0010	0.0016207	0.00161970	0.0016216	0.0016206	0.0016207	0.0016197	0.0016207	0.00161970
0.0001	0.0006673	0.00066690	0.0006672	0.0006668	0.0006673	0.0006669	0.0006673	0.00066690
0.00001	0.0005130	0.00057150	0.0005717	0.0005714	0.0005130	0.0005715	0.0005130	0.00057150

Table 17
The comparison of the values Q between BVP4c, DTM, LDTM, and GDTM.

	BVP4c		DTM		LSDTM		GDTM	
$\mathcal{Y}_a$	$m=0$	$m=1$	$m=0$	$m=1$	$m=0$	$m=1$	$m=0$	$m=1$
0.2	0.4435515	0.4434063	0.4436815	0.4438285	0.4435515	0.4434063	0.4435515	0.4434063
0.4	0.2671066	0.2670066	0.2670366	0.2670742	0.2671066	0.2670066	0.2671066	0.2670066
0.8	0.0340335	0.0340154	0.0340331	0.0340151	0.0340335	0.0340154	0.0340335	0.0340154

Table 18
The comparison of the values Q between BVP4c, DTM, LDTM, and GDTM

	BVP4c		DTM		LSDTM		GDTM	
$\mathcal{Y}_s$	$m=0$	$m=1$	$m=0$	$m=1$	$m=0$	$m=1$	$m=0$	$m=1$
0.2	−0.001849	−0.001848	−0.001849	−0.001848	−0.001849	−0.001848	−0.001849	−0.001848
0.4	−0.001849	−0.001848	−0.001849	−0.001848	−0.001849	−0.001848	−0.001849	−0.001848
0.8	−0.001854	−0.001852	−0.001854	−0.001852	−0.001854	−0.001852	−0.001854	−0.001852

Table 19
Comparison between LSDTM and other methods when $C=0, \mathcal{Y}_a=0, \mathcal{Y}_s=0, G=0.036, m_2=0.09, N_c=0.1, N_r=0, \eta_G=0.2, B=0$ and $\varepsilon=\frac{\pi}{2}$

ξ	Displayed Results				Absolute Errors		
ξ	BVP4	LSDTM	NARX-LMA [32]	CFB-LMA [33]	$\mathbf{Error_{LDTM}}$	$\mathbf{Error_{NARX-LMA}}$	$\mathbf{Error_{CFB-LMA}}$
0.0	1.000000000	1.000000000	0.99995159	0.99999448	0.0000000	4.8×10^{-5}	5.50×10^{-6}
0.1	0.97597354	0.975973530	0.97597345	0.97597344	1.1×10^{-8}	9.0×10^{-8}	1.00×10^{-7}
0.2	0.957555098	0.957555088	0.95755500	0.95755498	1.0×10^{-8}	9.8×10^{-8}	1.18×10^{-7}
0.3	0.944540825	0.944540811	0.94454070	0.94454070	1.4×10^{-8}	1.2×10^{-7}	1.25×10^{-7}
0.4	0.936788335	0.936788321	0.93678825	0.93678823	1.4×10^{-8}	8.5×10^{-8}	1.05×10^{-7}
0.5	0.934213456	0.934213441	0.93421384	0.93421334	1.5×10^{-8}	3.8×10^{-7}	1.16×10^{-7}

3.2 The Discussion of Graphics

i. The effect of differences in surface emissivity parameter and power index on thermal distribution

In Figure 4 and Figure 5 show how changes in surface emissivity B and power index m affect the fin's temperature distribution respectively. It is clear from Figure 4 that the power index and the rate of temperature drop of the porous fin are directly related. The fin has a constant coefficient of heat transfer is indicates by $m=0$, whereas heat transfer coefficient with a porous fin that depends on the temperature is indicated by $m>0$. Consequently, when the value of the power index increases,

so does the temperature of the fins. The thermal rate of loss is greatest for trapezoidal-shaped fins, then rectangular and dovetail profiles. Additionally, Figure 5 illustrates how differences in B affect the temperature distribution $\mathcal{Y}(\xi)$ of a longitudinal porous fin. Higher emissivity parameter values have been shown to be correlated with lower thermal distributions. Due to the fact that surface emissivity and temperature are closely correlated, when B increases, more heat is lost by radiation, which causes the temperature distribution of the fin to quickly drop. Therefore, higher B values translate into a quicker rate of heat transfer. In comparison to a dovetail profile fin followed by, a rectangle profile fin the trapezoidal profiled fin retains a lower thermal profile.

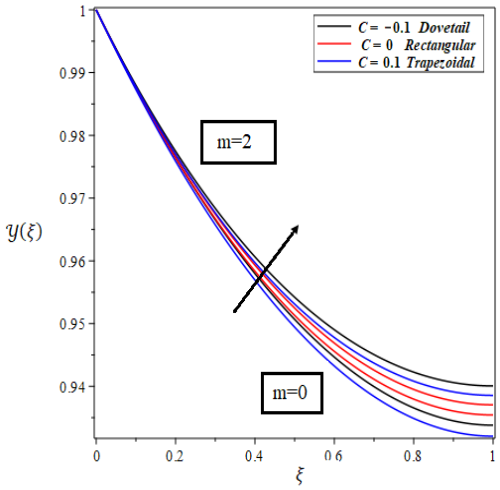

Fig. 4. Impact of changes in the power index m when $\mathcal{Y}_a = 0.5\,, \mathcal{Y}_S = 0.5\,, G = 0.1, m_2 = 1,$ $N_c = 1\ N_r = 1, \eta_G = 0.2\,, B = 0.2$ and $\varepsilon = \frac{\pi}{2}$

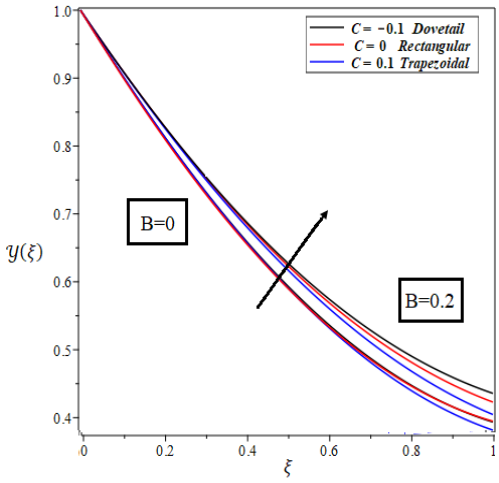

Fig. 5. Impact of changes surface emissivity parameter B when $\mathcal{Y}_a = 0.5\,, \mathcal{Y}_S = 0.5\,, G = 0.1, m_2 = 1, N_c = 1\ N_r = 1, \eta_G = 0.2$ and $\varepsilon = \frac{\pi}{2}$

ii. The effect of differences in sink temperature and ambient temperature on thermal distribution

In Figure 6 and Figure 7 correspondingly depict the impact on the thermal distribution of various strictures of the inclined longitudinal fin with modifications in sink temperatures $\mathcal{Y}_s$ and the dimensionless ambient $\mathcal{Y}_a$. These figures shown that rising ambient temperature and sink temperature are negatively to the fin cooling process because the raise in $\mathcal{Y}_a$ decrease the temperature differential between the fin surface and the surrounding air, which decreases natural convection. In fin this leads the rate of thermal drop is subsequently decreased. In a similar manner, higher sink temperatures reduce radiative heat loss. Thus, smaller values of $\mathcal{Y}_a$ and $\mathcal{Y}_s$ are therefore desired in both cases. Furthermore, the effects are the same for all three profiles (rectangle, dovetail, trapezoidal).

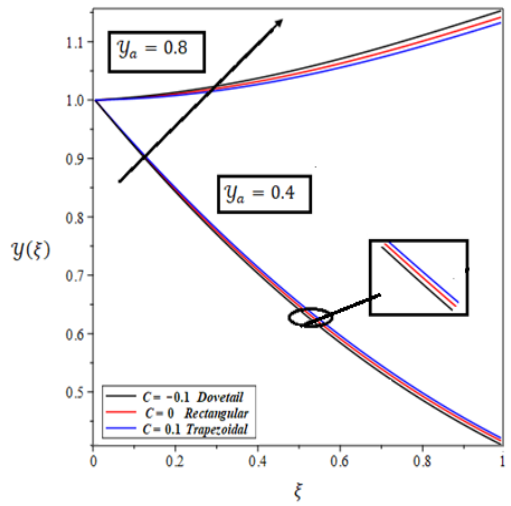

Fig. 6. Impact of changes in ambient temperature $\mathcal{Y}_a$ when $\mathcal{Y}_S = 0.2\,, G = 0.1, m_2 = 1, N_c = 1\ N_r = 1, \eta_G = 0.2\,, B = 0.2$ and $= \frac{\pi}{2}$

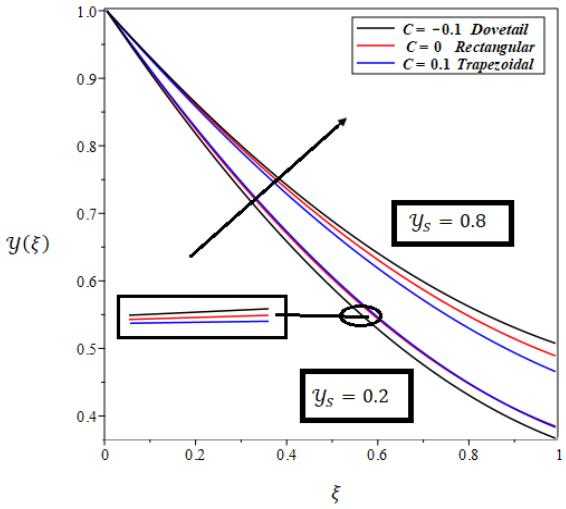

Fig. 7. Impact of changes in sink temperature when $\mathcal{Y}_a = 0.2\ , G = 0.1, m_2 = 1, N_c = 1$ $N_r = 1, \eta_G = 0.2$ and $\varepsilon = \frac{\pi}{2}$.

iii. The effect of differences in angle of inclination and wet porous parameter on thermal distribution

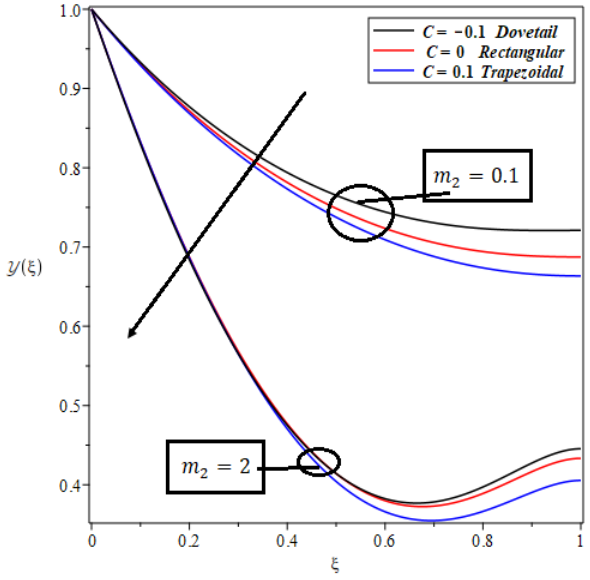

Fig. 8. Impact of changes in wet porous parameter m_2 when $\mathcal{Y}_a = 0.5\,, \mathcal{Y}_S = 0.5\,, G = 0.1, N_c = 1,\ N_r = 1 \eta_G = 0.2\,, B = 0.2$ and $= \frac{\pi}{2}$

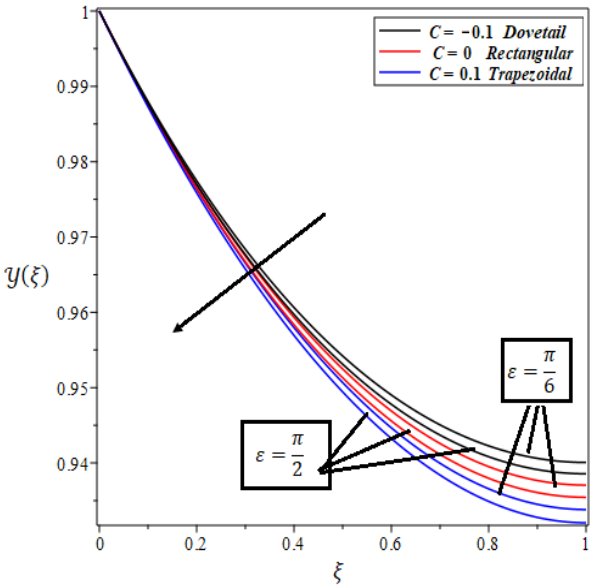

Fig. 9. Impact of changes in angle of inclination ε when $\mathcal{Y}_a = 0.5\,, \mathcal{Y}_S = 0.5\,, G = 0.1, m_2 = 1, N_c = 1\ N_r = 1, \eta_G = 0.2$

In Figure 8 and Figure 9 shown the wet porous parameter m_2 with angle of inclination ε affected the thermal profile of the completely porous fin. The temperature of the fin is shown to decline more quickly as the value of m_2 rise in Figure 8. This arises as a result of the increased loss of heat by convection caused by the porous surface area of the fins. Increased porosity parameter values are therefore recommended for hastening heat dissipation. Figure 9 displays how the temperature profile along the fin is influenced by the degree of inclination ε rising the tilt angle has a positive

impact on the fin's cooling process, according to the data. The temperature drops progressively from the base of the fin to the tip as the angle of inclination rises, acting as a driving factor for heat loss through convection. In light of this, a high inclination angle is required for the optimum fin.

iv. The effect of differences in dimensionless radiative parameter and progressive natural convection parameter on thermal distribution of a fin

In the inclined porous fin, the temperature distribution for various profiles that are deteriorating are shown in Figure 10 and Figure 11 under the impact of changes in dimensionless radiative parameter N_r and the progressive natural convective parameter N_c. It is essential to remember that N_c denotes the quality of heat transported from convection to conduction. The temperature surrounding the fin tip rapidly drops as the values of N_c grow because the fins lose heat more quickly in Figure 10. The temperature decreases as N_r grows over the whole length of the porous fin, as shown in Figure 11, since the radiative parameter N_r measures the intensity of surface radiation directed against the conductor. A rise in its value quickens the rate of heat transfer and intensifies radiative heat loss. The values greater of the dimensionless radiative parameters are therefore preferred for faster heat loss.

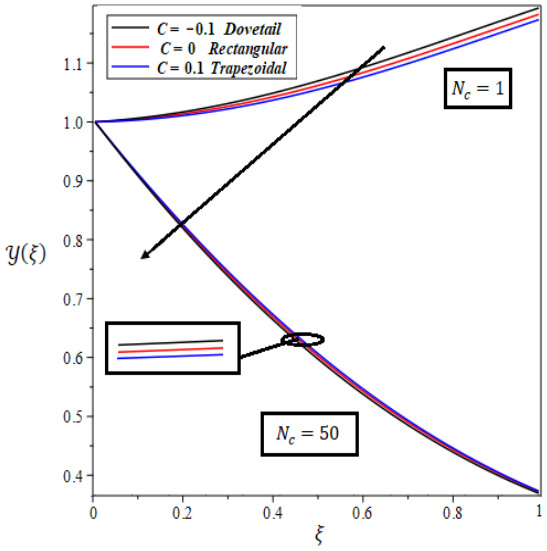

Fig. 10. Impact of changes in parameter N_c. when $\mathcal{Y}_a = 0.5$, $\mathcal{Y}_S = 0.5$, $G = 0.1, m_2 = 1$ $N_r = 1, \eta_G = 0.2$, $B = 0.2$ and $\varepsilon = \frac{\pi}{2}$

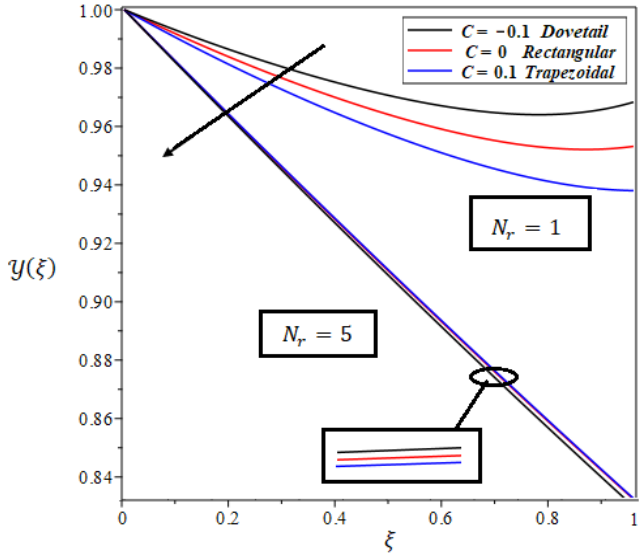

Fig. 11. Impact of changes in surface N_r when $\mathcal{Y}_a = 0.5$, $\mathcal{Y}_S = 0.5$, $G = 0.1, m_2 = 1$ $N_c = 1, \eta_G = 0.2$ and $\varepsilon = \frac{\pi}{2}$

v. The effect of differences in generating parameter on thermal distribution of a fin

In Figure 12 illustrates how the generating parameter G affects the temperature profile of the fin. In this situation, it is demonstrated that temperature is an increasing function of the producing parameter. This is due to the fact that when the producing parameter rises, more heat is produced inside the fin, which has a negative impact on the process of heat loss. Smaller values of the G hence assist in cooling the fins.

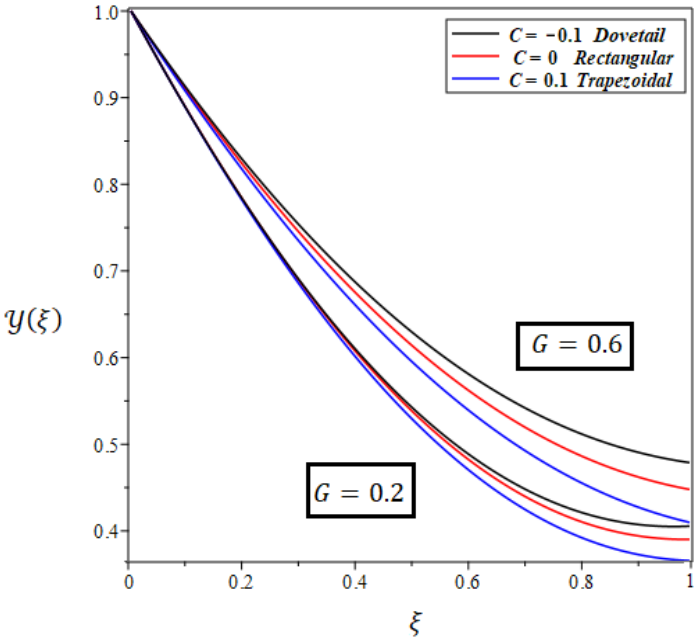

Fig. 12. Impact of changes generating parameter when $\mathcal{Y}_a = 0.5$, $\mathcal{Y}_S = 0.5$, $m_2 = 1$, $N_r = 1$, $\eta_G = 0.2$, $B = 0.2$, $N_c = 1$ and $\varepsilon = \frac{\pi}{2}$

4. Conclusions

In this study, the mathematical model of an inclined longitudinal fin has the analytical and numerical solutions of trapezoidal, dovetail, and rectangular forms under radiative and convective conditions are presented. The BVP4c and the optimal differential transform method are employed to discuss temperature distribution and the rate of heat transfer in the fin. These methods are used to investigate the impacts of changes in progressive natural convective parameter, the inclination angle, wet porous parameter, tip tapering, internal heat generation, dimensionless radiative parameter, porosity on heat transfer rate of various profiles and the thermal profile of the fin. The conclusion can be point in the following as:

i. In fins, the study of the graphic shows that surface emissivity, radiation, and convection all contribute to the heat loss rate.
ii. The optimal differential transfer method gives better results than the differential transfer method.
iii. The fin tip temperature is negatively impacted by the power index, the generation of heat parameter, sink temperature, and the ambient temperature.
iv. The wet porous parameter aid and the inclination angle in the fin's cooling process.
v. Comparing trapezoidal fins to rectangular and dovetail designs, they have a reduced thermal profile.
vi. The dovetail fin shape, followed by rectangular and trapezoidal fin profiles, has the highest rate of heat transfer.

Acknowledgement
This research was not funded by any grant.

References

[1] Vafai, K .“Heat Transfer of Nanofluids in Porous Media.” In *Handbook of Porous Media, Third Edition*, 491–92. CRC Press, 2015.

[2] Nield, Donald A., and Adrian Bejan. “Mechanics of Fluid Flow through a Porous Medium.” In *Convection in Porous Media*, 1–35. Cham: Springer International Publishing, 2017.

[3] Panchal, Hitesh, and Ravishankar Sathyamurthy. "Experimental analysis of single-basin solar still with porous fins." *International Journal of Ambient Energy* 41, no. 5 (2020): 563-569. https://doi.org/10.1080/01430750.2017.1360206.

[4] Queipo, Nestor V., and Efrain Nava. "A gradient boosting approach with diversity promoting measures for the ensemble of surrogates in engineering." *Structural and Multidisciplinary Optimization* 60, no. 4 (2019): 1289-1311. https://doi.org/10.1007/s00158-019-02325-4.

[5] Kiwan, Suhil. "Effect of radiative losses on the heat transfer from porous fins." *International journal of thermal sciences* 46, no. 10 (2007): 1046-1055. https://doi.org/10.1016/j.ijthermalsci.2006.11.013.

[6] Kundu, Balaram, and Dipankar Bhanja. "An analytical prediction for performance and optimum design analysis of porous fins." *International Journal of Refrigeration* 34, no. 1 (2011): 337-352. https://doi.org/10.1016/j.ijrefrig.2010.06.011.

[7] Gorla, Rama Subba Reddy, and A. Y. Bakier. "Thermal analysis of natural convection and radiation in porous fins." *International Communications in Heat and Mass Transfer* 38, no. 5 (2011): 638-645. https://doi.org/10.1016/j.icheatmasstransfer.2010.12.024.

[8] Petroudi, Rahimi Iman, Domairry Davood Ganji, Bahram Amir Shotorban, Khazayi Mehdi Nejad, Ehsan Rahimi, Reza Rohollahtabar, and Fatemeh Taherinia. "Semi-analytical method for solving non-linear equation arising of natural convection porous fin." *Thermal Science* 16, no. 5 (2012): 1303-1308. https://doi.org/10.2298/tsci1205303p.

[9] Kundu, Balaram, Dipankar Bhanja, and Kwan-Soo Lee. "A model on the basis of analytics for computing maximum heat transfer in porous fins." *International Journal of Heat and Mass Transfer* 55, no. 25-26 (2012): 7611-7622. https://doi.org/10.1016/j.ijheatmasstransfer.2012.07.069.

[10] Abdulridah, Saja Isam, and Abeer Majeed Jasim. "New Analytical Study of Heat Transfer Analysis of Jeffery–Hamel Nanofluid Flow Problem with Porous Medium." *Journal of Advanced Research in Fluid Mechanics and Thermal Sciences* 103, no. 1 (2023): 105-132. https://doi.org/10.37934/arfmts.103.1.105132.

[11] Aziz, A., and Mohsen Torabi. "Convective-radiative fins with simultaneous variation of thermal conductivity, heat transfer coefficient, and surface emissivity with temperature." *Heat Transfer—Asian Research* 41, no. 2 (2012): 99-113. https://doi.org/10.1002/htj.20408.

[12] Patel, Trushit, and Ramakanta Meher. "Thermal Analysis of porous fin with uniform magnetic field using Adomian decomposition Sumudu transform method." *Nonlinear Engineering* 6, no. 3 (2017): 191-200. https://doi.org/10.1515/nleng-2017-0021.

[13] Patel, Trushit, and Ramakanta Meher. "Thermal Analysis of porous fin with uniform magnetic field using Adomian decomposition Sumudu transform method." *Nonlinear Engineering* 6, no. 3 (2017): 191-200. https://doi.org/10.1515/nleng-2017-0021.

[14] Jawairia, Shahzadi, and Jawad Raza. “Optimization of Heat Transfer Rate in a Moving Porous Fin under Radiation and Natural Convection by Response Surface Methodology: Sensitivity Analysis.” *Chemical Engineering Journal Advances* 11, no. 100304 (2022): 100304. https://doi.org/10.1016/j.ceja.2022.100304.

[15] Roy, Pranab Kanti, Hiranmoy Mondal, and Bipattaran Raj. "Analytical and numerical solution of the longitudinal porous fin with multiple power-law-dependent thermal properties and magnetic effects." *Heat Transfer* 51, no. 3 (2022): 2702-2722. https://doi.org/10.1002/htj.22421.

[16] Jasim, Abeer Majeed. "Exploration of No-Slip and Slip of Unsteady Squeezing Flow Fluid Through a Derivatives Series Algorithm." *Journal of Advanced Research in Fluid Mechanics and Thermal Sciences* 100, no. 1 (2022): 11-29. https://doi.org/10.37934/arfmts.100.1.1129.

[17] Zhou, J. K. "Differential transformation and its applications for electrical circuits." (1986).

[18] Kundu, Balaram, Ranjan Das, and Kwan-Soo Lee. "Differential transform method for thermal analysis of exponential fins under sensible and latent heat transfer." *Procedia Engineering* 127 (2015): 287-294. https://doi.org/10.1016/j.proeng.2015.11.370.

[19] Sowmya, G., and Bijjanal Jayanna Gireesha. "Analysis of heat transfer through different profiled longitudinal porous fin by differential transformation method." *Heat Transfer* 51, no. 2 (2022): 2165-2180. https://doi.org/10.1002/htj.22394.

[20] Khudair, Ayad R., and S. A. M. Haddad. "Restricted fractional differential transform for solving irrational order fractional differential equations." *Chaos, Solitons & Fractals* 101 (2017): 81-85. https://doi.org/10.1016/j.chaos.2017.05.026.

[21] Hussin, Che Haziqah Che, Arif Mandangan, Amirah Azmi, and Adem Kilicman. "Solitary Wave Solutions for Forced Nonlinear Korteweg-de Vries Equation by Using Approximate Analytical Method." *Journal of Advanced Research in Fluid Mechanics and Thermal Sciences* 99, no. 2 (2022): 197-206. https://doi.org/10.37934/arfmts.99.2.197206.

[22] Varun Kumar, R. S., G. Sowmya, Fadl A. Essa, B. C. Prasannakumara, M. Alsehli, and B. Saleh. "RETRACTED: Thermal analysis of an annular fin under multi-boiling heat transfer coefficient using differential transform method with Pade approximant (DTM-Pade)." *Proceedings of the Institution of Mechanical Engineers, Part E: Journal of Process Mechanical Engineering* (2022): 09544089221076255. https://doi.org/10.1177/09544089221076255.

[23] Sabdin, Abdul Rahman Farhan, Che Haziqah Che Hussin, Arif Mandangan, Graygorry Brayone Ekal, and Jumat Sulaiman. "Approximate Analytical Solutions for Non-linear Telegraph Equations with Source Term." *Journal of Advanced Research in Applied Sciences and Engineering Technology* 31, no. 3 (2023): 238-248.

[24] Yaghoobi, Hessameddin, and Mohsen Torabi. "The application of differential transformation method to nonlinear equations arising in heat transfer." *International Communications in Heat and Mass Transfer* 38, no. 6 (2011): 815-820. https://doi.org/10.1016/j.icheatmasstransfer.2011.03.025.

[25] Beleri, Joonabi, and S. Kotnurkar Asha. "Peristaltic transport of Ellis fluid under the influence of viscous dissipation through a non-uniform channel by multi-step differential transformation method." *Journal of Advanced Research in Numerical Heat Transfer* 9 (2022): 1-18.

[26] Hussin, Che Haziqah Che, Arif Mandangan, Amirah Azmi, and Adem Kilicman. "Solitary Wave Solutions for Forced Nonlinear Korteweg-de Vries Equation by Using Approximate Analytical Method." *Journal of Advanced Research in Fluid Mechanics and Thermal Sciences* 99, no. 2 (2022): 197-206. https://doi.org/10.37934/arfmts.99.2.197206.

[27] Kiwan, Suhil. "Thermal analysis of natural convection porous fins." *Transport in porous media* 67 (2007): 17-29. https://doi.org/10.1007/s11242-006-0010-3.

[28] Ghasemi, S. E., P. Valipour, M. Hatami, and D. D. Ganji. "Heat transfer study on solid and porous convective fins with temperature-dependent heat generation using efficient analytical method." *Journal of Central South University* 21 (2014): 4592-4598. https://doi.org/10.1007/s11771-014-2465-7.

[29] Eshan, Abdul Rauf, and Wah Yen Tey. "Investigation of Shape Parameter for Exponential Weight Function in Moving Least Squares Method." *Progress in Energy and Environment* (2017): 17-24.

[30] Qayyum, Mubashir, Hamid Khan, M. Tariq Rahim, and Inayat Ullah. "Analysis of unsteady axisymmetric squeezing fluid flow with slip and no-slip boundaries using OHAM." *Mathematical Problems in Engineering* 2015 (2015). https://doi.org/10.1155/2015/860857.

[31] Meher, Ramakanta, and Nirav D. Patel. "Analytical Investigation of MHD Jeffery–Hamel flow problem with heat transfer by differential transform method." *SN Applied Sciences* 1, no. 7 (2019): 656. https://doi.org/10.1007/s42452-019-0632-z.

[32] Patel, N., and Ramakanta Meher. "Analytical investigation of Jeffery-Hemal flow with magnetic field by differential transform method." *Int. J. Adv. Appl. Math. Mech* 6 (2018): 1-9.

[33] Khan, Naveed Ahmad, Muhammad Sulaiman, and Fahad Sameer Alshammari. "Heat transfer analysis of an inclined longitudinal porous fin of trapezoidal, rectangular and dovetail profiles using cascade neural networks." *Structural and Multidisciplinary Optimization* 65, no. 9 (2022): 251. https://doi.org/10.1007/s00158-022-03350-6